Investigation of Hydrodynamic Forces on Articulated Concrete Block Mattresses in Fluid Flow from Various Horizontal Directions

by

Rory William Girven McLaren, BE (Ocean Engineering)

National Centre for Maritime Engineering and Hydrodynamics

Australian Maritime College, University of Tasmania

Submitted in fulfilment of the requirements for the Masters of Philosophy (Maritime Engineering)

University of Tasmania and Australian Maritime College

March 2019

Declaration of Originality

This thesis contains no material which has been accepted for a degree or diploma by the University or any other institution, except by way of background information and duly acknowledged in the thesis, and to the best of my knowledge and belief no material previously published or written by another person except where due acknowledgement is made in the text of the thesis, nor does the thesis contain any material that infringes copyright.

Authority of Access

This thesis may be made available for loan and limited copying and communication in accordance with the Copyright Act 1968.

Supervisory Team

Role:	Name:	Signature:
Candidate:	Rory McLaren	
Principal Supervisor:	Christopher Chin	
Second Supervisor:	Joshua Weber	
Third Supervisor:	Jonathan Binns	
Fourth Supervisor:	Dev Ranmuthugala	

Acknowledgments

I extend my acknowledgements to the following people, the AMC technicians including Michael Underhill, Rowan Frost and Tim Lilienthal, for their technical expertise and their help with experimental testing methodology. The other SUBCON research students, Murphy McColl and his tireless work, without which this project never would have come together. To Viet Lee Hung for his tireless efforts in creating the computational model. To Christopher Chin for his tireless input and constant supervision, without him none of this would have been possible. Jonathan Binns, for his technical expertise and boundless knowledge. Josh Weber for his practical knowledge and assistance during testing. To Dev Ranmuthugala for his technical writing advice. To Matthew Allen for his words of wisdom and industry knowledge.

Table of Contents

Table of Figures

Table of Tables

Abstract

This thesis investigates the optimisation of hydrodynamic stability for Articulated Concrete Mattress (ACM), to improve the cost efficiency of ACMs currently used in industry and enhance ACM stability calculations. ACMs are mainly deployed for subsea structure stabilisation and scour protection. They are most commonly used for subsea pipelines, but are also used in a range of other offshore and coastal applications. ACMs are currently sized in industry using roughly estimated hydrodynamic coefficients and large safety factors to account for the uncertainty in the coefficients. The large safety factors cause drastically increased stability requirements and therefore increase the required cost for each mattress. The aim of this thesis is to decrease the required safety factors by investigating the hydrodynamics of ACMs using novel investigation methods to find more accurate coefficients for industry stability calculations. This thesis also compares various existing block types to determine how variations in ACM block shape affect hydrodynamic stability. Additionally, this thesis will recommend shape optimisations to increase mattress stability and therefore increase cost efficiency.

The most effective method for investigating hydrodynamic coefficients is an experimental investigation using a scale model or a full-scale model. The stability of ACMs was investigated through several full-scale experimental investigations at the Australian Maritime College's (AMC's) Circulating Water Channel (CWC). The experimental investigations are split into three separate investigations. The first investigation determines the mattress failure location for all incident flow angles, thereby reducing the variables that are needed to be investigated in further testing. The second investigation compares several existing block types to determine their stability and allow for further optimisation of ACM block shapes and sizes. The third

investigation analyses the flow around current ACMs and recommends block optimisation along with current shape strengths and weaknesses.

The first two sections involve the acquisition of hydrodynamic coefficients with respect to variations in incident current angles. The experimentally acquired hydrodynamic coefficients are then input into a static stability calculation to determine the failure mechanism, location and velocity. To accurately define the failure mechanism of an ACM, the mattress failure location is first investigated. Literature shows that the leading-edge row has far lower stability than any other row of blocks within the ACM. However the failure position within the leading-edge row is not thoroughly investigated. This thesis compares the corner block to the centre block in the leading-edge, concluding that the centre block has lower stability for almost all flow angles and is therefore the earliest mattress failure location in the leading edge row. Through this comparison, further investigations are made more efficient by leaving only the centre block as the necessary point of investigation.

Due to this narrowing of the subject matter, several extra ACMs could be investigated. The second stage of this thesis investigates the comparison between three different ACM block types, the 300-series, the 400-series and the 500-series, which are variations of the same base block type. While the 300 and 500-series blocks are symmetrical about the horizontal plane, the 400-series has the bottom half of the 300-series and the larger top half of the 500-series, allowing for simple comparisons between the different block types. From the investigation, it is found that the 400-series has higher stability than the heavier 500-series. Due to its size, the 500-series costs more than the 400-series. Therefore purely based on hydrodynamic stability, the 500-series is obsolete when compared to the 400-series.

To improve upon the 400-series' shape efficiency, it is important to analyse which fluid mechanisms cause the 400-series' high stability. The third section of this thesis uses experimental and numerical investigations to analyse flow patterns around ACMs. Through these investigations it is found that the 400-series has a stable block shape due to its smaller and more streamlined bottom shell which reduces lift and its sheer top face which increases down force, thus creating an overall reduction in lift. These same factors also increase the drag component of the overturning moment. While drag force is still important, the reduction in lift has a greater effect on stability than the reduction in drag. From this thesis, it is found that an efficient block shape has higher pressures on the top shell than on the bottom shell. It is recommended that the bottom shell of the ACM be hydrodynamically optimised to achieve the most efficient increase in stability.

Nomenclature

Symbol	Description	Units
A_D	Cross sectional area perpendicular to the drag force.	m^2
A_L	Cross sectional area perpendicular to the lift force.	m^2
C_D	Drag coefficient.	-
C_L	Lift coefficient.	-
C_{OVT}	Overturning moment coefficient.	-
C_{OVT_A}	Overturning moment coefficient A.	-
C_{OVT_B}	Overturning moment coefficient B.	-
F_D	Drag force.	N
F_L	Lift Force.	N
H	Block height.	m
M_A	Overturning moment A.	Nm
M_B	Overturning moment B.	Nm
M_{OVT}	Overturning moment.	Nm
v	Velocity.	m/s
$v_{Failure_A}$	Failure velocity A.	m/s
$v_{Failure_B}$	Failure velocity B.	m/s
V	Volume.	m^3
$W_{Submerged}$	The submerged weight of one block.	N
ρ	Water density at the flume tank.	kg/m^3

Chapter 1

1 Introduction

1.1 Background

This thesis investigates the hydrodynamic stability of ACMs in fluid flow of varying incident angles. ACMs are a commonly used scour protection method, which are widely used for pipeline protection and stabilisation. ACMs are made up of a matrix of concrete blocks interconnected with wires or ropes. This increases the stiffness of the overall mattress while allowing for a flexible structure which can be laid over assets, as shown in Figure 1. The interconnections in the mattress improve the stability of the entire mattress. ACMs are also commonly anchored to the seabed at each corner of the mattress for added stability. ACMs are an efficient and cost effective asset stabilisation method due to their strength to weight ratio, which is created through the use of articulated joints between individual concrete blocks (McLaren, 2014).

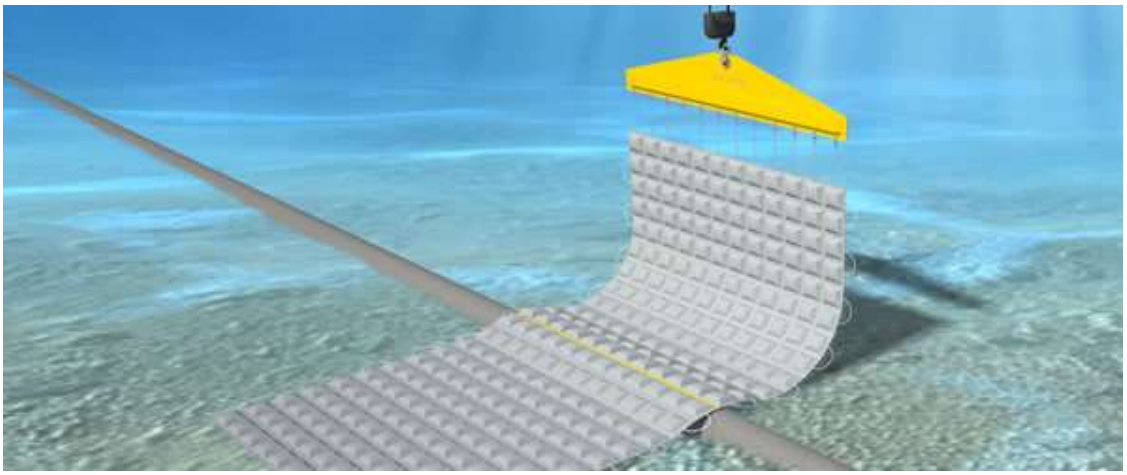

Figure 1: Articulated mattresses placed over a pipeline, (Seabed Technologies LLC, n.d.).

To ensure ACMs are effective for each project, a stability analysis must be conducted to appropriately size the ACM. A summary of the design methodologies and stability analysis of ACMs in industry is described in Godbold (2014). There are several standards that are currently used for mattress stability such as *DNV* (1988) and *DNV* (2007). While these are both well respected and provide reasonable methods for scour protection stability analysis, neither use hydrodynamic coefficients found through experimental or numerical analysis. Instead they use estimated coefficients from other subsea structures. As stated by Griggs (2014), "*almost no studies have previously been published which describe the hydrodynamic forces experienced by these mattresses"*. Due to the uncertainty within the coefficients, large safety factors are used to conduct mattress stability analyses. These large safety factors can result in unnecessary costs and inefficient design.

Previous studies have been undertaken to determine coefficients for ACM blocks at the Australian Maritime College (AMC) by Chrenowski (2014), McLaren (2014), Francis (2013),

Carnovale (2014), Arzaghi (2014), Lau (2014) and Lim (2013). Also, Griggs (2014) conducted some research at Edith Cowan University (ECU). However to date, only a single block type has been tested at two flow angles using a consistent methodology. This limits the knowledge of ACM hydrodynamic stability due to the inability to accurately compare the results of these findings.

Griggs (2014) investigated the 500-series, shown in Figure 2, at incident flow angles of 0º and 45º. However, intermittent angles are not included within Griggs (2014)'s scope and therefore there is a knowledge gap around the incident flow angle with the highest hydrodynamic coefficient. Corner block stability, and therefore the failure location, is also outside of Griggs (2014)'s scope. Francis (2013) investigated several different block locations and found that within the leading edge of the mattress, the corner block has the lowest hydrodynamic coefficients. However, Francis (2013)'s paper only investigated an incident flow angle perpendicular to the leading-edge. While perpendicular flow to the leading edge is hypothetically the lowest stability flow angle for the centre block, the corner block hypothetically is in its highest stability flow direction. Consequently, further investigations are needed to find the failure location and block type comparisons.

1.2 Scope

The scope of this thesis is to conduct experimental and theoretical investigations to find hydrodynamic coefficients and the failure velocity for each of the ACM block types. The goal is to obtain a relationship between flow velocity, block type and incident flow angle. From these findings, this thesis will simplify the identification of the failure flow velocity for application in the maritime industry. Along with procuring the failure velocity of existing block types, this research will investigate the fluid mechanics that improves mattress stability and

propose possible improvements to the block shape to generate a superior mattress weight to stability ratio.

Section 5.2 of this thesis investigates how hydrodynamic loads vary with block location. By investigating the initial failure location of the mattress, the required data for each block type can be reduced to one block location. The investigation is done by comparing the stability of the corner block and the centre block on the leading-edge at all horizontal incident flow angles, to determine which block has the lowest stability.

To ensure the validity of the experiments several repeated incident flow angles were investigated. The incident flow angles range between 0º and 45º, with repeating angles of -15º and 60º for validity. The incident flow angle -15º is used to check the repeatability of the results as it will have identical coefficients to 15º. The incident flow angle 60º was tested to validate the assumption that the leading edge is the lowest stability block location. If 45º has higher stability than 60º then the mattress side edge must be investigated. This range of incident flow angles covers all mattress failure conditions.

Section 5.3 follows on from the block location analysis by investigating different block types and how varied block sizes affect mattress stability. Three different block types in six different flow angles will be tested. The ACM block types that are experimentally tested will be the 300-series, 500-series and 400-series, which are depicted in Figure 2. Each block is the combination of two half blocks, the bottom half and the top half. The 400-series is made up of the bottom half of the 300-series and the top half of the 500-series. Testing the 400-series will allow for an investigation into how the variation in the half shells affects mattress stability.

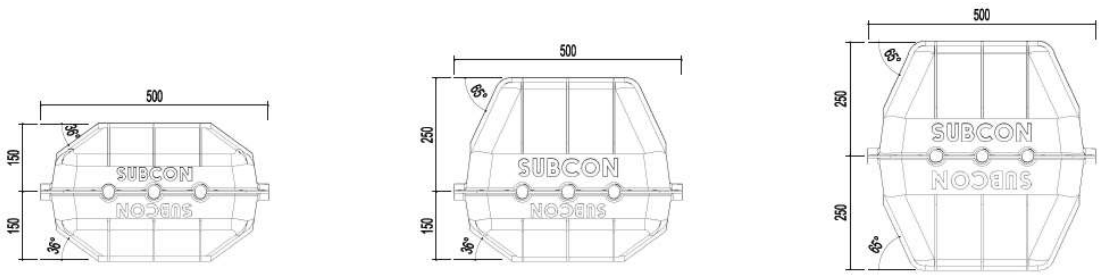

Figure 2: The Subcon Technologies block types, the 300-series, 400-series and 500-series respectively.

This thesis also seeks to determine the dominant fundamental flow mechanism that causes mattress failure, as investigated in Section 6.4. By analysing the flow mechanisms around ACMs and comparing these findings to the stability results found in Section 5.2 and 5.3, design improvements can be made through intelligent design and further hydrodynamic investigations. Once a detailed ACM mattress flow profile is built, further investigations can be undertaken into the causes of mattress failure. A detailed failure assessment will also allow for localized optimisation of block shape. By optimizing the shape of blocks, a more cost-efficient block can be implemented.

1.3 Objective Statement

This thesis seeks to answer the question, what is the influence of incident flow angle and block shape on the stability of an ACM and what improvements could be made to existing block shapes? To determine the stability of each different block type, the ACM failure location must first be investigated. The research is split up into three major components. Section 5.2 investigates the stability of a full mattress and how block position within a mattress affects the stability of the block at different flow angles. By defining the main failure location within the

mattress, Section 5.2's conclusions simplify further investigations into different block types. Section 5.3 seeks to investigate the effect of the block type on mattress stability and recommends existing block types with high stability to cost ratios. Section 6.4 investigates local hydrodynamic effects around the blocks and links these effects to the stability of the mattresses found in the previous two sections. Through this investigation, the strengths and weaknesses of ACMs can be developed thus allowing for future block advancements.

1.4 Implications of Research

This thesis seeks to find ACM hydrodynamic coefficients that could be used by industry to increase the accuracy of their ACM stability analyses. The block comparison will clarify which block types are more economical and will help in deciding which block type to choose for specific deployment sites. Research into the strengths and weaknesses of the block shape will allow for further block optimisations in the future, which will allow for more economical block shapes. The findings of this thesis will also open further opportunities for the investigation of hydrodynamic forces on ACMs in the future.

1.5 Outline of Thesis

Rory McLaren's three research papers have been combined and structured to form this classic format thesis, which are broken down into the following chapters.

Chapter 2 is a review of previous works on the analysis of ACM stability through hydrodynamic modelling using experimental analyses, numerical investigations and fluid modelling.

Chapter 3 discusses the methods used in the testing. First, a detailed explanation of the experimental setup is given. This includes how the model is setup, positioned in the flume tank and the testing equipment. Next, the test procedure is discussed followed by the steps necessary to reduce the data and perform drag, lift, and overturning moment acquisition using the 6 degrees of freedom load cell.

Chapter 4 outlines the method for processing the data acquired and obtaining the drag coefficient, lift coefficient and failure flow rates. This chapter also goes into the theory behind ACM flow mechanics.

Chapter 5 presents the results of the study. Figures are presented that show the failure flow rates of the mattresses.

Chapter 6 discusses the results of Chapter 5. Later in this chapter, there is a flow mechanics investigation with several figures showing the flow profile around the ACM..

Chapter 7 summarizes the study and formulates conclusions and recommendations based on the results in Chapter 5 and discussions in Chapter 6.

Chapter 2

2 Literature Review

Localised scour has been a major concern since the 1950s and earlier, though much of the research only started in the early 1970s. In the 1950s, localised scour was brought to the attention of the public due to several studies into the effect of scour on bridge failures. As discussed by Deng (2010), localised scour around structures such as bridge piers (Figure 3) can cause significantly reduced structural stability and even lead to structural failures if not accounted for. Between 1950 and 1991, Shirhole (1991) surveyed 823 bridge failures and found that 60% of the failures were due to scour.

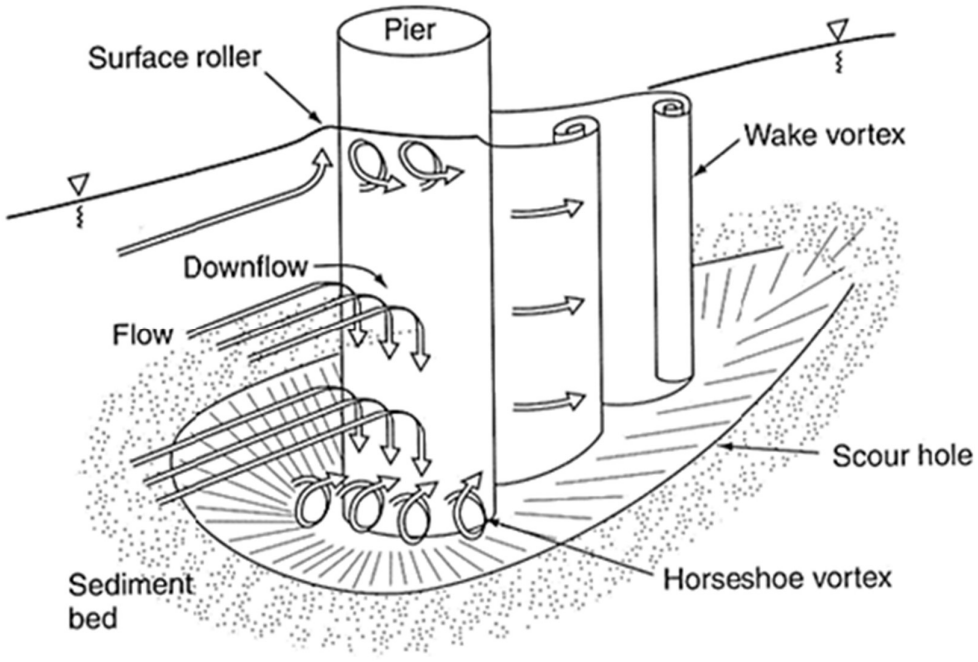

Figure 3 : Localised scour at the base of pile structures (Deng, 2010)

The cost associated with repairing these bridges spurred dramatically, encouraging research into localised scour around bridges based in New Zealand. Between 1972 and 1994, 37 research papers were written on the topic as shown in Melville (2000).

The negative effect of scour on coastal and nearshore structures life spans are discussed in Hales (1980) and Lillycrop (1993). They discovered that scour is one of the major factors in the reduction of service life and increase in maintenance costs of coastal and nearshore structures.

Pipelines are a more recent marine structure, with all major pipelines being constructed in the last 40 years. Pipelines are subject to major scour, which creates unsupported sections of the pipeline, called free spans. Free spans can cause the pipeline to locally buckle in the middle of the free span causing major economic and environmental problems (Sumer, 2002). Figure 4 shows unprotected scour propagation along a subsea pipeline.

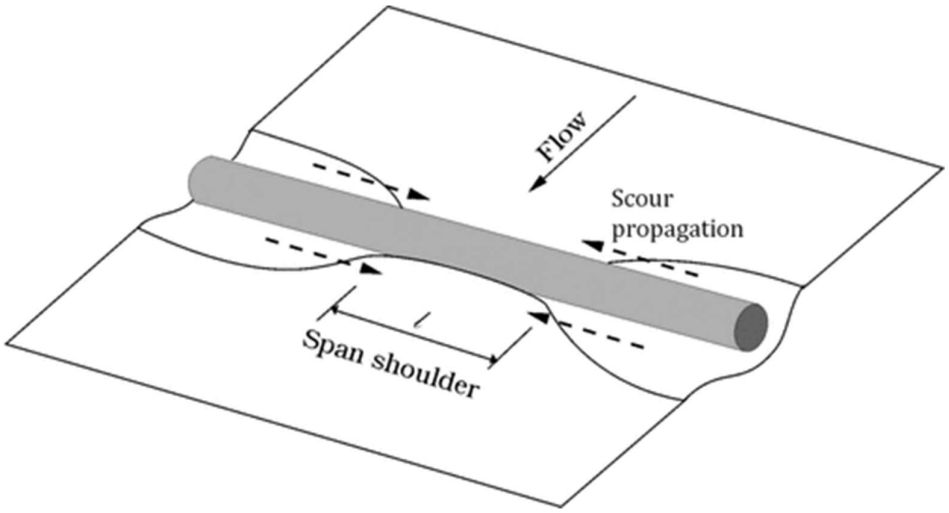

Figure 4 : Free span scour propagation (Fredsøe, 2016).

Major research into pipeline scour started in the early 1970s. Sumer (1988), Sumer (1991), Klomp (1995) and Sumer (2001) investigated the onset of scour under pipelines. Kjeldsen (1973), Lucassen (1984) and Sumer (1990) investigated the expansion of scour holes and the process that creates free spans. Sumer (2002) further summarises the early stages of investigations into pipeline scour.

Several pipeline protection strategies have been engineered to stop free span failures from occurring as found in the standards of *DNV* (1988) and *DNV* (2007). These pipeline protection methods are split into two major sections, free span rectification and scour protection. Free span rectifications involve surveying the pipeline and implementing a hard structure, such as a grout bag or rocks, to support the middle of the free span. Alternatively, scour protection involves protecting the pipeline from scour in the first place. This can be done by pipeline burial or scour protection mattresses. One of the most common types of scour mattresses are ACMs. Scour under pipelines is the main reason ACMs were invented and therefore scour mitigation is key for any design choices made for ACMs.

A summary of the design methodologies and stability analysis of ACMs in industry is described by Godbold (2014). Other helpful design papers are Dunlap (2001), Lagasse (2007) and *NCMA* (2010). These papers help in the design and development of a general scour protection mattress. They do not delve into the specific stability of ACMs, which is needed to accurately size an appropriate ACM for a specific environment.

The industrial standards used for calculating mattress stability are *DNV* (1988) and *DNV* (2007). While these are well respected and reasonable methods for scour protection, the scope of these standards is limited to standard shape coefficients and do not include ACM hydrodynamic coefficients. As stated by Griggs (2014), there are very few published studies

that describe the hydrodynamic forces experienced by ACMs. Due to the uncertainty within the standard hydrodynamic coefficients, large safety factors are used to conduct mattress stability analyses. This leads to unnecessary costs and thus produce inefficient designs.

Previous studies have been undertaken to find coefficients for ACM blocks at the Australian Maritime College (AMC) by Chrenowski (2014), McLaren (2014), Francis (2013), Carnovale (2014), Arzaghi (2014), Lau (2014) and Lim (2013). Francis and Lim studied the 300-series ACM in 2013 and found that the corner block has lower lift and drag coefficients than the centre block at a flow angle of 0° as seen in Figure 5. Francis and Lim's scopes were limited to only fluid flow perpendicular to the leading edge. It was found that the corner block exhibits lower forces than the centre block for perpendicular flow.

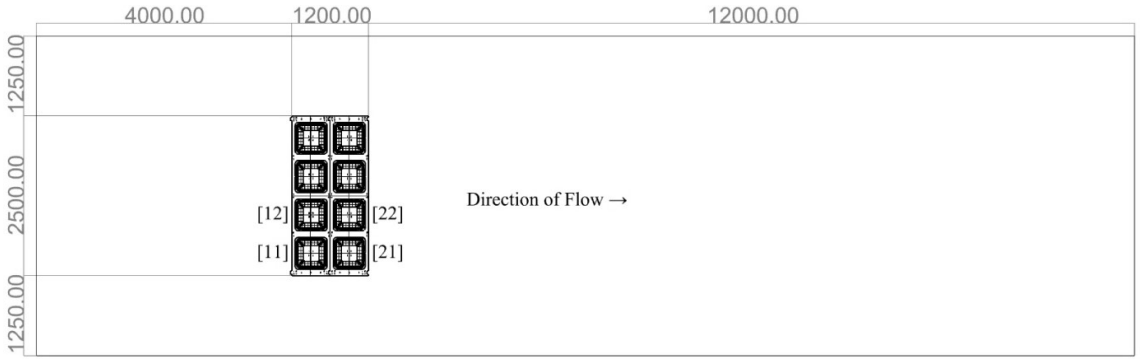

Figure 5: Francis and Lim 300-series mattress arrangement Francis (2013).

Chrenowski (2014), McLaren (2014), Carnovale (2014), Arzaghi (2014) and Lau (2014) compared experimental to theoretical and numerical methods for conducting stability analyses on ACM revetments. In revetments, it was found that the leading edge has the lowest stability when compared to blocks at the free surface and blocks placed on a slope. However, this study's scope was limited to a single block type (500-series) at a flow angle of 0°.

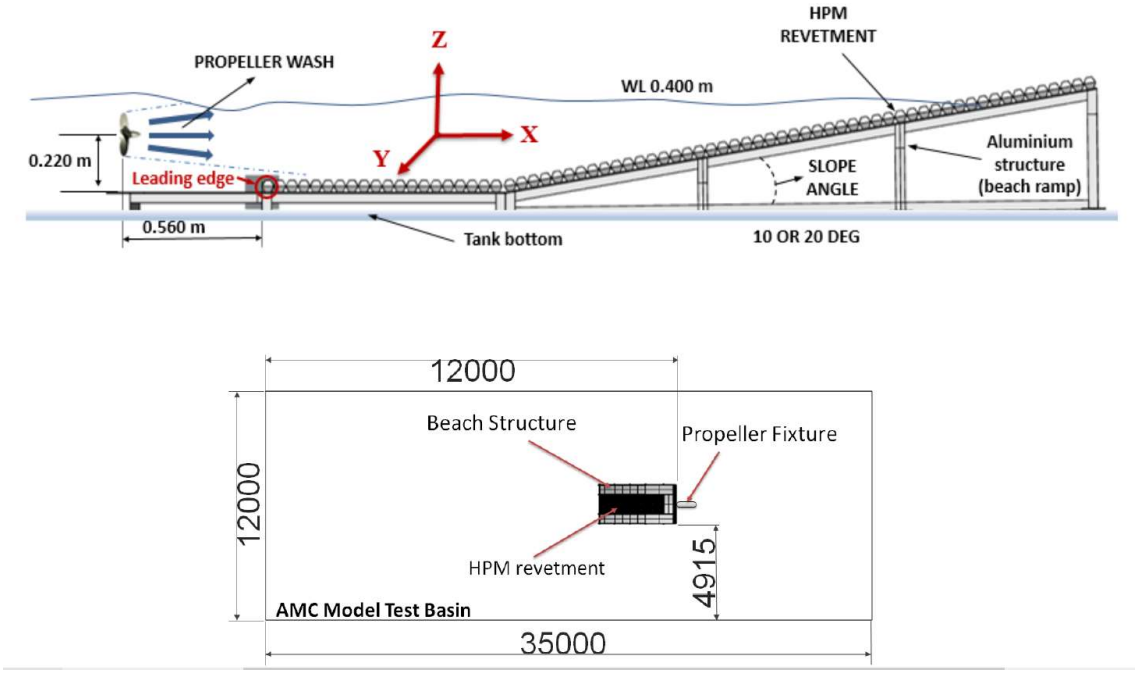

Figure 6: Schematic of the experiment set up: The top drawing shows the model set up and the coordinate systems adopted for the experiment. The bottom drawing shows the position of the model in the basin (Chrenowski, 2014).

Griggs (2014) evaluated the 500-series, as shown in Figure 2, at fluid angles of 0º and 45º. Intermittent angles were outside of Griggs (2014)'s scope. Therefore, the maximum flow coefficients for flow angle is a knowledge gap from past literature.

This thesis aims to reduce the knowledge gaps in past literature. The knowledge gaps this thesis aims to covers are how intermittent incident flow angles and block shape affects ACM hydrodynamic coefficients. In conjunction with this thesis, McColl (2016), Taylor (2016) and Neville and McLaren (2016) all conducted similar experimental investigations. McColl (2016) experimentally investigated the 300-series mattress at various incident flow angles, Taylor (2016) investigated the effect of a dramatically shortened bottom shell by comparing the block types investigated in this thesis to blocks with a 50mm high bottom shell. Neville and McLaren

(2016) investigated the effect of flipping the 400-series upside down, effectively raising the separation point of a block with the same weight and height.

Chapter 3

3 Method

3.1 Introduction

The experimental phase of this research project is made up of several full-scale experimental investigations into the effects of fluid flow on ACMs, specifically ACM hydrodynamic forces and how they affect mattress stability. Additionally, an experimental study into the flow profile around an ACM is conducted in conjunction with the CFD investigation by Hung (2016).

3.2 Testing Tank Specifications

The model was tested in AMC's Circulating Water Channel (CWC) which is also commonly known as a flume tank. The CWC is a current based tank that is 11m by 5m by 2.5m deep. The CWC is usually used for fishing nets and various other experimental models, including midwater arches, hydrofoils, Remotely Operated Vehicle (ROV) and Autonomous Underwater Vehicle (AUV) testing. The tank itself has a rotating belt that allows for free stream velocity throughout the tank. This belt is turned off for this experiment thereby allowing a full boundary layer to form.

3.3 Model Specifications

The experimental model used in this research project was designed by Francis (2013) and consists of a large steel base plate that holds the blocks in place, as shown in Figure 7. One of the novel components of this thesis is the development of the model to hold 3 blocks, so that a

3 by 3 mattress can be tested. The model's base plate is now 2.5 metres long by 1.8 metres wide. This novel methodology allows for simulated centre block studies as well as the edge block studies conducted by Francis (2013).

Figure 7: Experimental model made up of a large steel base plate that holds a 3 by 3 mattress fixed in place. The model is now 2.5 metres long by 1.8 metres wide.

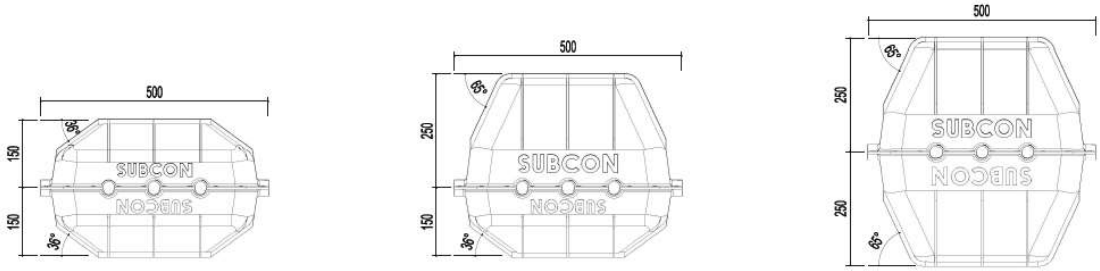

Figure 8: The Subcon Technologies block types, the 300-series, 400-series and 500-series respectively.

The plastic shells were supplied by Subcon Technologies, which are the precise block shapes used in industry as shown in Figure 8. These blocks are all 500mm by 500mm wide and a height signified by name, for example the 300 series is 300mm high. The blocks must be placed with minimal spacing between them to accurately imitate ACMs used in industry. However, the load cell block must always have a small gap between it and its neighbouring blocks to record accurate results. This spacing must be repeatedly checked throughout the testing. If the blocks were found to be touching at any point in the testing process, then the previous tests were repeated. The blocks are pinned to the steel plate through threaded bars to ensure minimal movement.

The only block not pinned in this way is the load cell block which has its own load cell frame as seen in Figure 9. This frame connects the block to the load cell. To position the load cell block just above the steel plate, steel packers are used to accurately raise the load cell block off the steel plate. This is performed at the start of every experiment to maximise the accuracy of the results. The blocks were also checked to ensure they were not touching the surrounding steel plate. Spacing between the block and the steel place is ensured by manually loading up the loadcell block and analysing the voltage output to check for any contact.

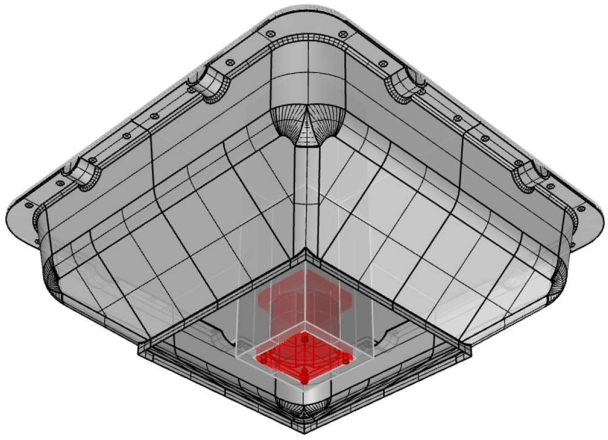

Figure 9: Underside view of load cell casing in mattress block. (Francis, 2013)

3.4 Instrumentation

The load cell used for this experiment was an AMTI SF3-SSUDW 250 pound six degrees of freedom load cell. The load cell is fully calibrated using a 6 by 6 cross talk matrix. A detailed description of a cross talk calibration is described by Schrand (2018). The cross talk calibration provided an improvement to the methodologies undertaken in past studies by Francis (2013), Chrenowski (2014), McLaren (2014) and Carnovale (2014), allowing for improved accuracy in the results of thesis. An example of a cross talk matrix from one of the experiments is shown in Table 1. To calibrate the load cell, the voltage to weight gradient is experimentally calculated by applying known weights to the load cell. Incrementally increasing the weight will give a constant gradient which is used as the calibration factor. This process is repeated for all 6 degrees of freedom. While applying a weight to an axis, the load cell voltage is recorded for all axes. This process is used to determine the accuracy of the load cell and how much cross talk can be expected during the experiment.

Table 1: Cross talk calibration matrix for the 500-series and 400-series.

K Matrix	Fx	Fy	Fz	Mx	My	Mz
Fz	0.333	0.067	-29.727	0.018	0.007	0.001
Fx	-7.721	-0.133	-0.174	0.005	-0.009	0.011
Mz	0.044	-0.332	0.236	-0.001	-0.001	0.209
My	0.046	0.057	-0.640	-0.004	0.143	0.002
Mx	-0.008	0.025	0.116	0.134	0.003	-0.001
Fy	0.091	8.007	-0.597	0.003	0.002	-0.024

3.5 Experimental Test Set-up

Following the assembly of the model and the calibration of the load cell, the experimental set-up was created. Prior to the model being placed in the CWC, several weights were arranged around the tank to ensure the conveyer belt did not lift in the fluid flow. These weights were all placed behind the model, to ensure the fluid flow was unobstructed.

Once all the weights were in place the model was moved to the middle of the tank by craning it onto the flume tank carriage. The model was then lowered into the CWC by crane. Special attention was made to ensure the load cell cables were clear of any moving parts. To ensure repeatability, the model was placed with the front middle of the steel plate in the centre of the tank. This was achieved by lining up the model with existing lines marked on the bottom of the tank and lining up the leading edge of the blocks with the Subcon ACM marker on the carriage rail. The conveyer belt was switched off before the CWC turbines were turned on to ensure no movement of the model.

3.6 Testing Program

Table 2 shows the testing regime for different angles. This process was repeated for all 6 different flow angles and each block. Each velocity was recorded for 3 minutes. Once a velocity

was recorded, the flow velocity was increased. Three minutes is required to allow for the flow velocity to stabilise before further runs are recorded. The velocity was increased to a maximum of 1.4 m/s and then reduced to 0 m/s to avoid the hysteresis effect, therefore decreasing inaccuracies.

The testing regime is repeated at -15, 0, 15, 30, 45 and 60 degrees (Figure 11), where 0 degrees is fluid flow perpendicular to the leading row of blocks, also known as the leading edge. These angles were tested for each different block type.

Table 2: Testing regime for each angle.

Run Number	Flow Velocity
1	0
2	0.4
3	0.4
4	0.6
5	0.6
6	0.8
7	0.8
8	1
9	1
10	1.2
11	1.2
12	1.4
13	1.4
14	1
15	0.6
16	0

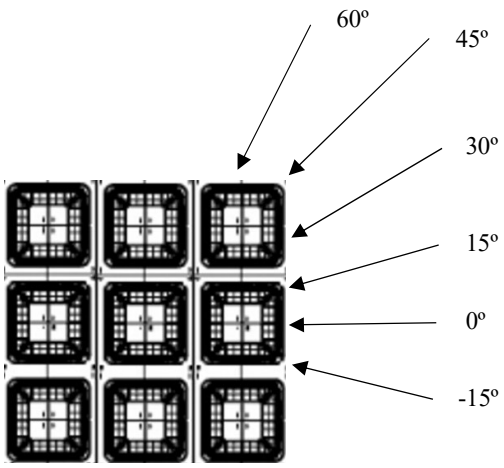

Figure 10: Testing regime, incident flow angles.

3.7 Experimental Procedure Data Acquisition

3.7.1 Three-Dimensional Flow Profiling Method

Two different three-dimensional flow profiling methods are investigated in this thesis. The first is an experimental investigation that uses streamlines to estimate the three-dimensional flow profile around an ACM. The second is a Computational Fluid Dynamics (CFD) investigation that considers detailed streamlines around an ACM to visualise the pressure distribution around the mattress.

3.7.1.1 Experimental Three-Dimensional Flow Profiling

To experimentally create a streamline flow profile around the 3 by 3 block mattress, strands of cassette tape were employed as shown in Figure 11. Cassette tape was utilised due to its neutral

buoyancy, flat face which allows it to more easily follow fluid flow compared to other materials like string and it is also very visible when used in hydrodynamic experiments.

To capture the flow profile a three-camera set-up was used. Two fixed cameras were placed at the front and back of the mattress, outside of the CWC Perspex window. The third camera was a Go-Pro which was used to capture close-ups and angles that the other two cameras could not achieve.

This form of flow profiling has been commonly used at the AMC. This form of experiment is exploited to evaluate boundary layer effects and to study areas of eddy generation. By investigating these fluid effects around the ACM, the mattress can be evaluated to identify areas of high and low pressure, thus validating how the shape of the mattresses affects its stability and how ACMs may be hydrodynamically enhanced.

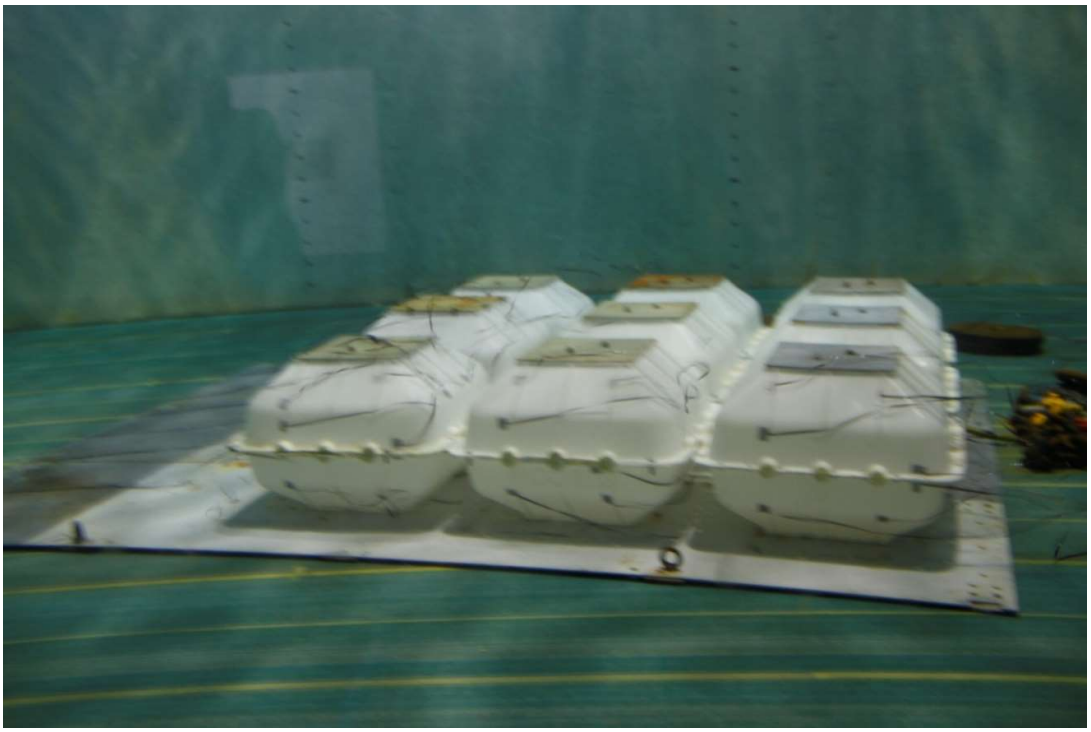

Figure 11: Experimental model in the CWC.

3.7.1.2 CFD Three-Dimensional Flow Profiling

Hung (2016) completed the CFD analysis used in this thesis by employing the Reynolds Averaged Navier-Stokes (RANS) method. The RANS method is conducted by using the finite volume solver ANSYS CFX, which simulates hydrodynamic effects on structures. The RANS method was used for the 300, 400 and 500-series ACM in the same three by three block mattress arrangement which was investigated in the experimental method. While Hung (2016) used ANSYS CFX to numerically investigate the hydrodynamic loads on ACMs, only the flow visualisation is investigated in this thesis. ANSYS CFX is a modelling software that is commonly used in hydrodynamic modelling.

While CFD is useful for the flow visualisation around ACMs, there are several differences between a numerical analysis and an experimental analysis. The experimental model has several imperfections, such as the base plate or the limited fluid domains size. However, the numerical model is based on approximations, resulting in inconsistencies in the boundary layer and the input flow profile.

3.8 Uncertainty Analysis

The following uncertainty analysis was conducted using a simple repeatability analysis of each set of results. The percent uncertainty for each resultant and its associated block type and location are shown below in Table 3 and Table 4 respectively. Uncertainties in the results of this thesis range from +3% -2% for the 400-series failure flow rate B to +30% -12% for the 300-series centre block's drag coefficient. A common cause of the uncertainty within the results of this study is due to the hysteresis effect, this effect is commonly seen most strongly when flowrates are being reduced near zero.

Table 3: Uncertainty ranges for each resultant and its associated block locations.

Block Location	Drag		Lift		Overturning		Failure Flow Rate A		Failure Flow Rate B	
300 Centre	30%	-12%	18%	-9%	22%	-8%	4%	-8%	4%	-9%
300 Corner	22%	-8%	17%	-9%	23%	-9%	5%	-8%	4%	-8%

Table 4: Uncertainty ranges for each resultant and its associated block type.

Block Type	Drag		Lift		Overturning		Failure Flow Rate A		Failure Flow Rate B	
500 Series	18%	-13%	23%	-12%	7%	-8%	6%	-8%	4%	-6%
400 Series	6%	-7%	17%	-9%	6%	-5%	5%	-8%	3%	-2%
300 Series	30%	-12%	18%	-9%	22%	-8%	4%	-8%	4%	-9%

A separate uncertainty analysis was conducted by comparing repeating angles of -15 and 15 degrees for the centre block and 30 and 60 degrees for the corner block. In theory, these angles should have identical results. However due to uncertainties within the experimental testing method, these angles have the percentage uncertainties as shown in the results section.

Chapter 4

4 Theory

4.1 Failure Mechanisms

To define the failure of each block type, it is important to determine the earliest failure mechanisms for the mattress itself. McLaren (2014) showed that there are three major failure mechanisms for ACMs, global lift, leading-edge lift and wave run-up. Wave run-up is only relevant to revetment mattresses, which are outside the scope of this thesis. Global blocks have higher stability than leading-edge blocks as discovered by Francis (2013) and Griggs (2014). This thesis expands upon their research by analysing the exact failure mechanism of an individual leading-edge block. Mattress failure is conservatively assumed to be any loss in static stability. This is assumed to account for increased lift once the fluid flow gets under the block. However, this ignores the mattresses increase in stability due to its articulated nature.

The leading-edge fails through overturning of the blocks, therefore the overturning moment shown in Figure 12 is investigated in addition to lift and drag. The overturning moment causes the leading-edge blocks to hinge around the connection with the second row of blocks. Pivot point A in Figure 12 represents the failure mechanism A. For option A to be a logical failure mechanism, it must be assumed that point A will act like a pin joint, therefore acting as a point of rotation. It is important to note that for both failure mechanisms the block overturns perpendicular to the front edge of the block and not in line with the fluid flow. This is different to most hydrodynamic testing where drag will be taken in line with the flow. For all results within this thesis, both drag and overturning moment will be in line with the mattress not with

the fluid flow. In addition to this fact all associated variables with drag and overturning moment are calculated in accordance with this directionality.

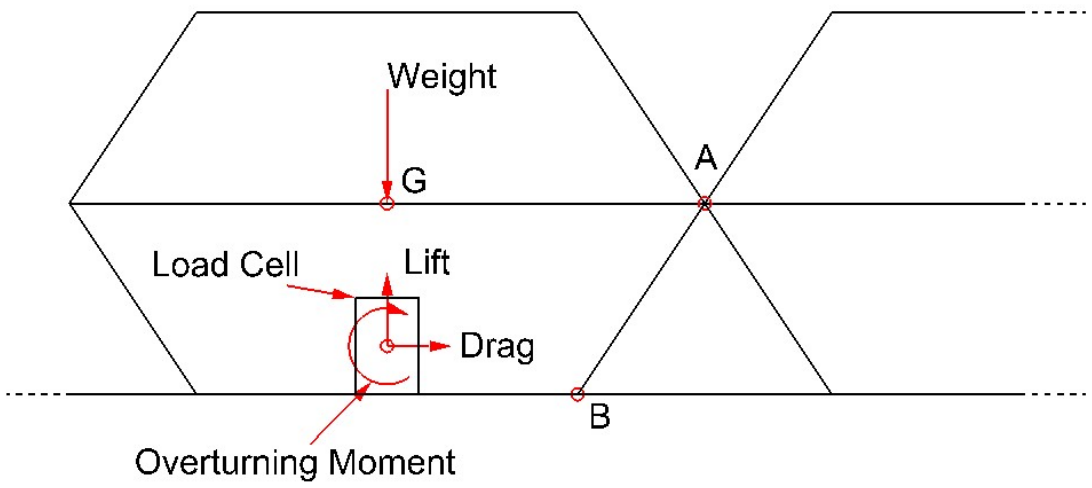

Figure 12: Overturning moment failure mechanisms.

An alternative failure mechanism occurs about point B is shown in Figure 12, which is used by Griggs (2014). This occurs when the connection between the blocks is loose enough to cause the leading-edge block to pivot about point B instead. These are referred to as failure method A and failure method B respectively. The failure method is dependent on the stiffness of the joint at A. The stiffness of connection A is variable depending on the materials used and construction consistency. Therefore, this thesis will compare the two failure mechanisms to identify the mechanism with the lowest failure velocity for use in stability analyses. The methodology chosen was conservative, however future research can be done to define the failure mechanism with more certainty.

4.2 Hydrodynamic Force Coefficients

The coefficients of drag and lift are a method of quantifying the resistance to fluid flow for a simple 2-dimensional or complex 3-dimensional shape. The typical equations to determine the coefficients of drag (C_D) and lift (C_L) from their respective forces are shown in Equations (1) and (2) respectively. To find the coefficients, each variable must first be measured. The coefficients are calculated from drag force (F_D), lift force (F_L), water density (ρ) at 999.1 kg/ m^3, fluid velocity (v), the cross-sectional area for drag (A_D) and the cross-sectional area for lift (A_L). These variables change depending on the environment and block type under investigation. However, A_D is constantly the cross-sectional area of the blocks in line with the front face of the mattress irrespective of the flow direction.

$$C_D = \frac{2F_D}{\rho v^2 A_D} \tag{1}$$

$$C_L = \frac{2F_L}{\rho v^2 A_L} \tag{2}$$

4.3 Overturning Moment Coefficient

Due to the importance of the overturning moment in calculating the failure mechanism of an ACM, a non-dimensional coefficient was created to describe the overturning moment. In its simplest form, the overturning moment is a combination between asymmetrical drag and lift about the centre of the load cell or about the point that acts as a hinge. ACM pivot points are defined in Section 4.1 as points A and B shown in Figure 12. Due to the units of the overturning moment, a projected area cannot be used in its hydrodynamic coefficient equation. Instead, it is proposed that the volume of the block (V) be used instead of a cross sectional area. Using

volume accounts for combined lift and drag directionality. Using the volume also keeps the coefficient as a non-dimensional number due to the moment's units of Nm. The overturning moment coefficient equation proposed is Equation (3). The overturning moment is represented by M_{OVT} and its corresponding coefficient is C_{OVT}.

$$C_{OVT} = \frac{2M_{OVT}}{\rho v^2 V} \tag{3}$$

4.4 Failure Velocity

The failure velocity is calculated when the fluid velocity in Equations (1), (2) and (3) create an overturning moment about the pivot point ($M_A \; or \; M_b$) equal to the restoring moment generated by the submerged weight of the block (W_{Sub}) as seen in Equations (4) and (5). The overturning moment found from the load cell is the moment about the centre of the load cell, and not the moment about the pivot points A and B.

The equations for the overturning moment coefficient about the pivot points A and B are shown in the derivations of Equations (4) and (5) respectively. These moments are derived by combining M_{OVT}, F_D and F_L at the loadcell and multiplying each force by its appropriate lever arm to find the sum of moments at the moment's respective axis. The moment shift to the pivot point at A involves the height of the block (H_{Bl}), width of the block ($w_{Bl} = 500mm$) and the height of the load cell ($H_{LC} = 76mm$). Only the block height is variable dependent on the block type. Moment B is dependent only dependant on ($H_{LC} = 76mm$) and the width of the base of the block ($w_{BlB} = 250mm$), both of which are constants. The pivot points A and B failure flow rate equations are shown in Equations (4) and (5) respectively. The failure flow

rate for pivot point A is denoted by ($v_{FailureA}$) and the failure flow rate for pivot point B is represented by ($v_{FailureB}$).

$$M_A = W_{Sub}\frac{w_{Bl}}{2}$$

$$M_A = M_{OVT} + F_L\frac{w_{Bl}}{2} - F_D\left(\frac{H_{Bl}}{2} - \frac{H_{LC}}{2}\right)$$

$$M_{OVT} + F_L\frac{w_{Bl}}{2} - F_D\left(\frac{H_{Bl}}{2} - \frac{H_{LC}}{2}\right) = W_{Sub}\frac{w_{Bl}}{2}$$

$$\frac{C_{OVT}\rho v_{Failure_A}^2 V}{2} + \frac{C_L\rho v_{Failure_A}^2 A_L}{2}\frac{w_{Bl}}{2} - \frac{C_D\rho v_{Failure_A}^2 A_D}{2}\left(\frac{H_{Bl}}{2} - \frac{H_{LC}}{2}\right) = W_{Sub}\frac{w_{Bl}}{2}$$

$$v_{Failure_A}^2\rho\frac{C_{OVT}V + 0.5C_L A_L w_{Bl} - 0.5C_D A_D H_{Bl} + 0.5C_D A_D H_{LC}}{2} = W_{Sub}\frac{w_{Bl}}{2}$$

$$v_{Failure_A}^2 = \frac{0.5W_{Sub}w_{Bl}}{0.5\rho(C_{OVT}V + 0.5C_L A_L w_{Bl} - 0.5C_D A_D H_{Bl} + 0.5C_D A_D H_{LC})}$$

$$v_{Failure_A} = \sqrt{\frac{W_{Sub}0.5}{\rho(C_{OVT}V + 0.5C_L A_L 0.5 - 0.5C_D A_D H_{Bl} + C_D A_D 0.076)}}$$

$$v_{Failure_A} = \sqrt{\frac{0.5W_{Sub}}{\rho(C_{OVT}V + 0.25C_L A_L - C_D A_D(0.5H_{Bl} - 0.038))}} \quad (4)$$

$$M_B = W_{Sub}\frac{w_{BlB}}{2}$$

$$M_B = M_{OVT} + F_L\frac{w_{BlB}}{2} + F_D\left(\frac{H_{LC}}{2}\right)$$

$$M_{OVT} + F_L\frac{w_{BlB}}{2} + F_D\left(\frac{H_{LC}}{2}\right) = W_{Sub}\frac{w_{BlB}}{2}$$

$$\frac{C_{OVT}\rho v_{Failure_B}^2 V}{2} + \frac{C_L\rho v_{Failure_B}^2 A_L}{2}\frac{w_{BlB}}{2} + \frac{C_D\rho v_{Failure_B}^2 A_D}{2}\left(\frac{H_{LC}}{2}\right) = W_{Sub}\frac{w_{BlB}}{2}$$

$$\rho v_{Failure_B}^2\frac{C_{OVT}V + 0.5C_L A_L w_{BlB} + 0.5C_D A_D H_{LC}}{2} = W_{Sub}\frac{w_{BlB}}{2}$$

$$v_{Failure_B}^2 = \frac{0.5W_{Sub}w_{BlB}}{0.5\rho(C_{OVT}V + 0.5C_L A_L w_{BlB} + 0.5C_D A_D H_{LC})}$$

$$v_{Failure_B} = \sqrt{\frac{W_{Sub}w_{BlB}}{\rho(C_{OVT}V + 0.5C_L A_L w_{BlB} + 0.5C_D A_D H_{LC})}}$$

$$v_{Failu\ \ _B} = \sqrt{\frac{W_{Sub}0.25}{\rho(C_{OVT}V + 0.5C_L A_L w_{BlB} + 0.5C_D A_D H_{LC})}}$$

$$v_{Failure_B} = \sqrt{\frac{0.25W_{Sub}}{\rho(C_{OVT}V + 0.5C_L A_L 0.25 + 0.5C_D A_D 0.076)}}$$

$$v_{Failure_B} = \sqrt{\frac{0.25W_{Submerged}}{\rho(C_{OVT}V + 0.038C_D A_D + 0.125C_L A_L)}} \quad (5)$$

4.5 Flow Mechanics

To investigate the three-dimensional flow mechanisms around ACMs, the flow profile can be broken down into individual fluid mechanics. Each of these effects follows fundamental fluid

mechanics and are combined into an overall understanding of ACM fluid mechanics. For hydrodynamic force investigations, it is important to fundamentally understand how ACM shape variations cause variations in the hydrodynamic loads applied to the mattress. For lift and drag, the fundamental fluid mechanic that produces the hydrodynamic load is the differential pressure around the structure, where lift is a vertical differential pressure and drag is a differential pressure in line with the fluid flow. Using the conservation of mass and momentum, the fluid velocity can be used to estimate the fluid pressure because velocity is inversely proportional to hydrodynamic pressure. While this method is an oversimplification for complex three-dimensional structures such as an ACM, if used cautiously, the conservatism of mass and momentum can be used to define the entire fluid system.

Using streamlines is a simple method for finding zones of pressure relief by observing patterns of cross flow as seen in front of the corner blocks in Figure 13. Possibly the most well-known example of pressure relief is wing tips. For a plane to fly, there must be a pressure imbalance between the top and bottom of the wing. A simple flat plate wing however has significant

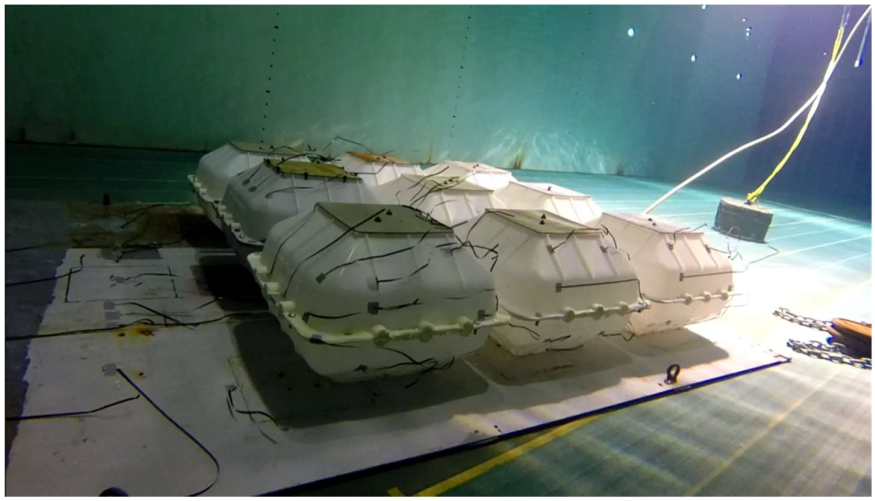

Figure 13: Experimental model with the 300-series attached, during testing in the CWC.

pressure relief at the tip of the wing, causing significant loss in lift. To combat this pressure loss, winglets were designed (Langevin, 2003). Unlike plane wings, ACMs need minimal lift and therefore pressure loss should be maximised, not reduced.

4.6 Complex Drag

One of the fundamental flow mechanisms of current on a submerged structure is complex drag. To properly analyse the drag acting on a structure, it is important to understand the type of drag that is acting on the structure.

Complex drag systems have several components such as form drag, skin friction and interference drag. Form drag, also known as pressure drag, is the drag component based on hydrodynamic shape and is induced from longitudinal differential pressure. This differential pressure creates an asymmetrical force system on the structure, therefore inducing a drag force. Skin friction is a simple frictional drag caused by the fluid passing along the surface of the block. While skin friction has significant effect on hydrodynamically efficient shapes such as wings, it has far less impact on hydrodynamically inefficient shapes due to the increased effect of form drag and interference drag. Interference drag is the force created due to the shift in fluid momentum when a fluid flow shifts around an object through the space that another object occupies. Interference drag is a subset of skin friction and form drag. The constricted flow at the base of the ACM induces high interference drag.

Chapter 5

5 Experimental Results

5.1 Introduction

The experimental results chapter of this thesis is split into two main sections. Section 5.2 investigates Articulated Concrete Mattress (ACM) failure locations by comparing the leading-edge centre block to the leading-edge corner block. The location comparison uses the 300-series ACM (a standard 300mm tall, symmetrical ACM) as the base model. The main aim of Section 5.2 is to find the lowest stability block location for use in the block type comparison of Section 5.3, where the main failure location found from Section 5.2 will be used to compare the 300-series to the 400-series (a standard 400mm tall ACM with a 250mm tall top shell and a 150mm tall bottom shell) and the 500-series (a standard 500mm tall, symmetrical ACM).

5.2 Block Location Investigation

This section investigates how hydrodynamic loads vary with block location. By investigating the initial failure location of the mattress, the required data for each block type can be reduced to one block location. The investigation is done by comparing the stability of the corner block and the centre block on the leading-edge at all horizontal incident flow angles, to determine which block has the lowest stability.

5.2.1 Coefficient of Lift

The coefficient of lift for the 300-series centre block and corner block comparison is shown in Figure 14. The centre block has higher lift than the corner blocks up to a flow angle of 30º, which is the maximum lift incident flow angle. Flow perpendicular to the mattress at 0º is the most commonly tested angle for ACMs, however it has the lowest lift coefficient. Previously, most studies investigated the lowest lift angle instead of the highest scenario. The corner block has a maximum lift at 45º and 60º and has a minimum lift at 0º.

The lift coefficient repeatability is high for both the centre and corner blocks. The flow angle of -15º has a slightly higher lift than 15º for the centre block giving a repeatability uncertainty of 3.52%. The flow angle of 60º for the corner block is slightly higher than 30º, also giving a

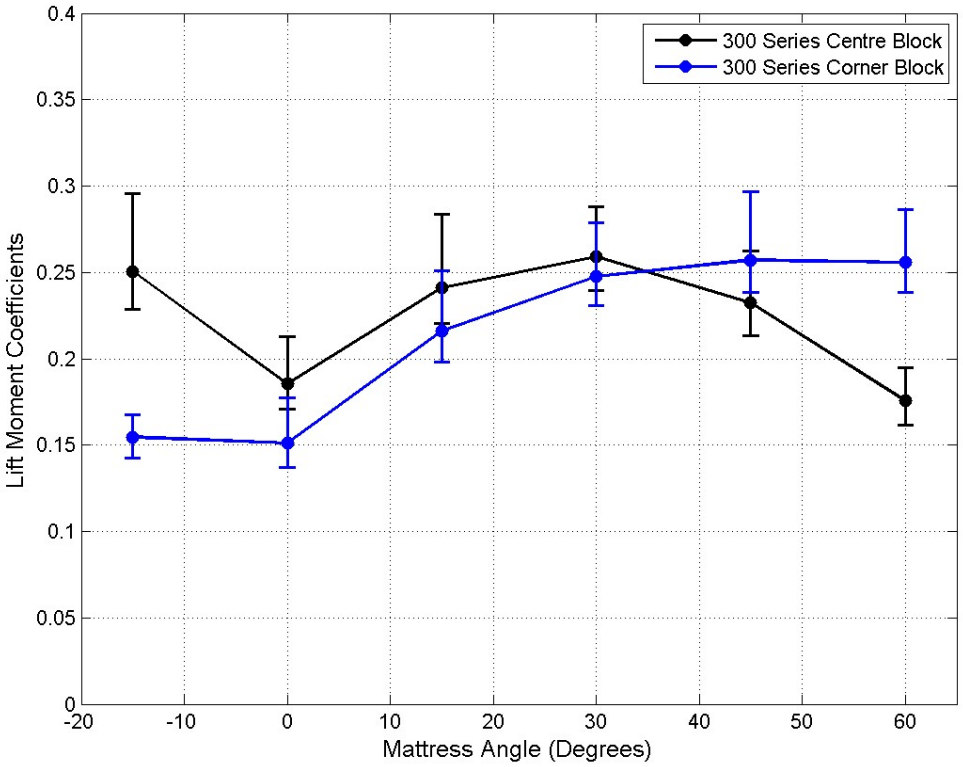

Figure 14: Lift coefficients for the 300-series centre and corner blocks.

repeatability uncertainty of 3.30%. The total uncertainty of the centre block lift results is +18% to -9%. The corner block has a peak uncertainty of +17% to -9%.

5.2.2 Coefficient of Drag

The coefficient of drag for the 300-series centre block and corner block comparison is shown in Figure 15. The drag coefficients for the centre block are higher than the corner block at angles lower than 30º. There is a repeatability uncertainty percentage of 4.80% between -15º and 15º for the centre block. The corner block however has a larger repeatability uncertainty of 17% between 30º and 60º. The total uncertainty of the centre block drag results is +30% to -12%. The corner block has a peak uncertainty of +22% to -8%.

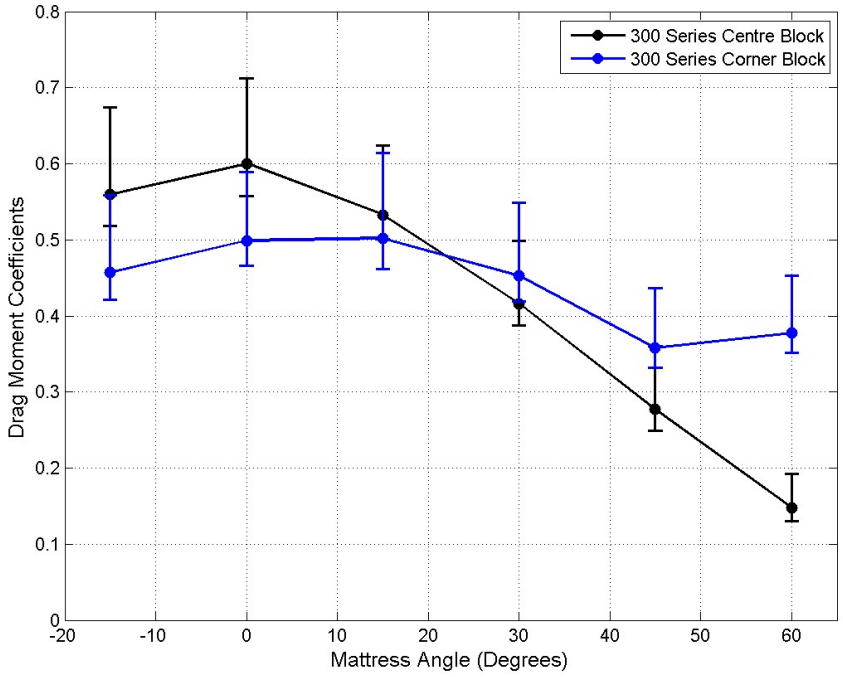

Figure 15: Drag coefficients for the 300-series centre and corner blocks.

5.2.3 Failure Velocity

The comparison of failure flow rate for method A acting on the 300-series centre block and corner block is shown in Figure 16. The failure flow rate is inversely proportional to the lift and overturning moment coefficients. At pivot point A, drag affects the overturning moment due to the location of the load cell below point A. Therefore, the drag coefficient has a proportional effect on the failure flow rate unlike the lift and overturning moment coefficients. However, failure velocity A shown in Figure 16 is dominated by the inversely proportional effect of lift.

When comparing these two block positions it is important to remember that regarding the failure of a full mattress for current in any direction, the hydrodynamic coefficients for flow angles 0° and 45° repeat around the full 360° of the mattress. This creates a repeating curve every 90°. Therefore, 60° is ignored when comparing these two block locations. The 300-series mattress fails due to the centre block losing stability and not due to the corner block. This

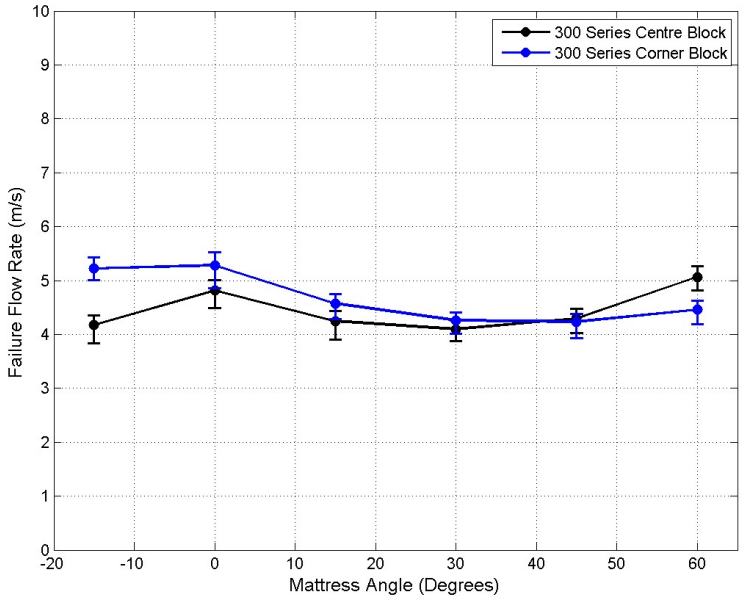

Figure 16: Failure flow rate for the 300-series centre and corner blocks, for failure method A.

means that the corner block can be disregarded when looking at full mattress stability. The centre block has a failure flowrate of 0.484m/s higher to 0.028m/s lower than the corner block (for values between 0º and 45º, the other two incident angles are only used for verification purposes). The repeatability for the failure flow rate is a combination between the errors of each of the previously investigated coefficients and therefore does not need further investigation. The total repeatability error is 1.61% between -15° and 15°. The flow angle of

60º for the corner block is slightly higher than 30º, also giving a repeatability uncertainty of 3.30%. The total uncertainty of the centre block failure flowrate A results is +4% to -8%. The corner block has a peak uncertainty of +5% to -8%.

The failure flow rate for method B acting on the 300-series centre block and corner block comparison is shown in Figure 17. In comparison to the failure flow rate about the pivot point A, drag instead has a positive influence on pivot point B. Here, the failure flow rate has an inverse relationship to the lift, drag and overturning moment coefficients. Furthermore, this positive effect caused by drag dramatically reduces the failure flow rate at low angles and therefore causes a far smaller minimum stability angle.

Considering the 300-series failure method B, the mattress fails from the centre blocks unless the angle is between 40º and 45º, in which case the corner block fails earlier. This means that for each repeating 45º section of the mattress, the corner block only fails before the centre block with incident flow angles directly at each corner. The corner block can be assumed to have negligible effect on mattress stability. This is due to the maximum difference between the failure flow velocities of the corner block in comparison to the centre block which is 0.1 m/s lower. The corner block will still need to lift the adjacent centre block. The centre block has a failure flowrate of 0.271m/s higher to 0.067m/s lower than the corner block (for values between 0º and 45º, the other two incident angles are inconsequential to mattress failure). The corner block's lower stability is negligible when considering the stability of a structure. Therefore, the focus of further research will be on the centre block instead of the corner block, as it is the main failure location. From analysing the repeatability of 15° and 15° the total uncertainty is 1.95% between -15° and 15°. The flow angle of 60º for the corner block is slightly higher than 30º,

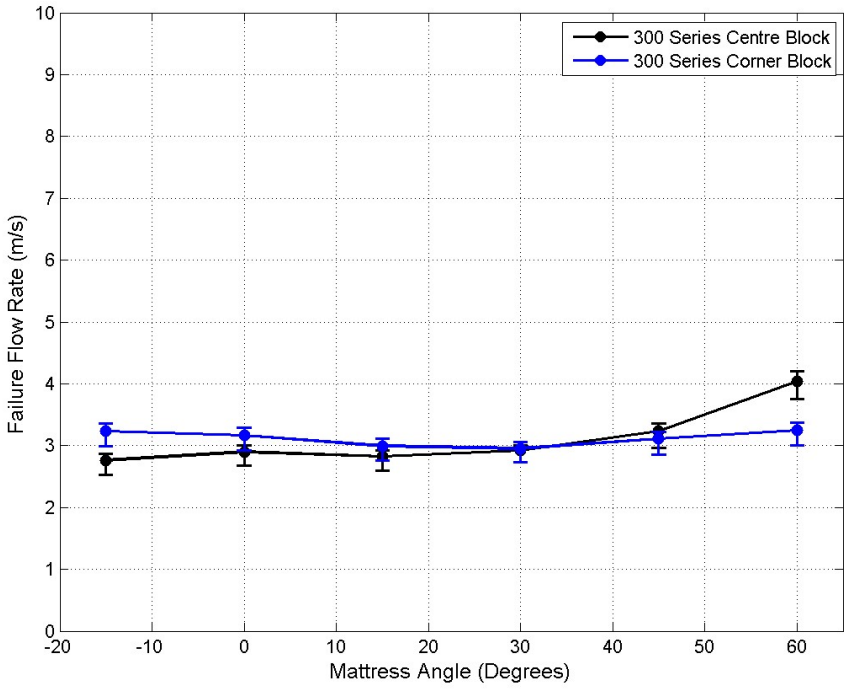

Figure 17: Failure flow rate for the 300-series centre and corner blocks, for failure method B.

also giving a repeatability uncertainty of 4.20%. The total uncertainty of the centre block failure flowrate A results is +4% to -9%. The corner block has a peak uncertainty of +5% to -8%.

5.2.4 Block selection

From this preliminary study, it is concluded that only the centre block of the other block types is needed to be tested in further investigations. This allowed for more thorough testing of the centre blocks in Section 6.4, which compares the 300-series, 400-series and 500-series mattresses. From this study it is recommended that in future ACM investigations outside of this thesis, only the centre block in the leading edge should be investigated. It is recommended that the mattress should be at least 3 blocks wide and at least 2 blocks long. However, if a study with a mattress of only 2 blocks long is conducted, a sensitivity study should be done to check for variations between a 2 and 3 block long mattress.

5.3 Block Type Comparison

This section follows on from the block location analysis by investigating different block types and how variations in block size affects mattress stability. Three different block types in six different flow angles will be tested. The ACM block types experimentally tested are the 300-series, 400-series and 500-series. Each block is the combination of two half blocks, the bottom half and the top half. The 400-series is in fact made up of the bottom half of the 300-series and the top half of the 500-series. Testing the 400-series will allow for an investigation into how the variation in the half shells affects mattress stability.

5.3.1 Coefficient of Lift

This section is an experimental comparison between the 300-series, 400-series and 500-series mattresses. It is insightful to compare the 400-series to the other block types as it can be assumed that the bottom half of the block is the half that affects the coefficient of lift. The top half has limited effect on the lift coefficient because the 400 and 300-series have almost identical lift coefficients as seen in Figure 18.

The 500-series has far greater lift than the 300-series and 400-series as seen in Figure 18. The 400 series has low lift relative to its size as it has equal or lower lift than the 300 series mattress.

The repeatability for the 300-series, 400-series and 500-series lift coefficient is 3.52%, 4.00% and 0.69% respectively by comparing the difference between -15° and 15°. The 500 series, 400

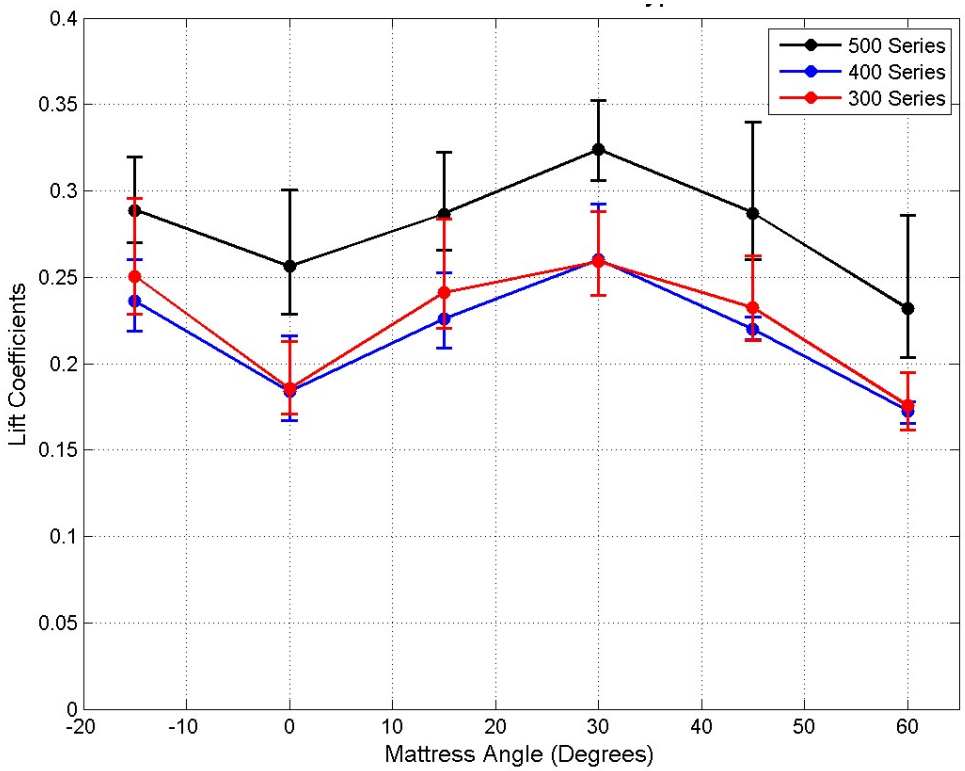

Figure 18: Lift coefficient for the 300-series, 400-series and 500-series centre blocks.

series and 300 series have peak lift uncertainties of +23% to -12%, +17% to -9% and +18% to -9% respectively.

5.3.2 Coefficient of Drag

Hydrodynamic coefficients including the drag coefficient are also known as shape coefficients because the size of the submerged object is accounted for in the cross-sectional area. With size accounted for, the only parameter that affects the coefficient is the block shape. As seen in Figure 19, the less streamline 500-series has a lower drag coefficient than both the 300-series and 400-series.

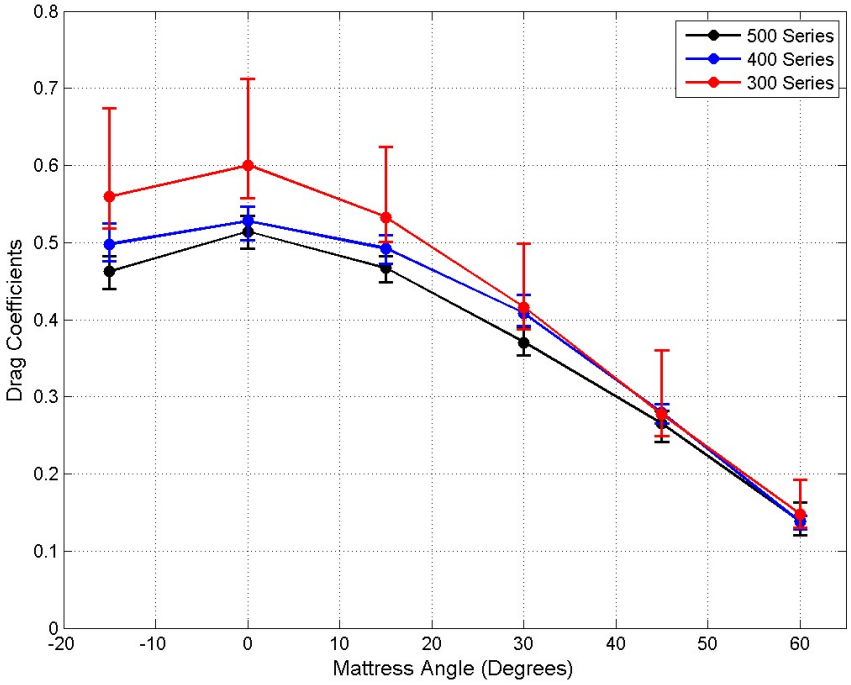

Figure 19: Drag coefficient for the 300-series, 400-series and 500-series centre blocks.

The repeatability for the 300-series, 400-series and 500-series drag coefficient is 4.80%, 1.38% and 0.71% respectively by comparing the difference between -15° and 15°. The 500 series, 400 series and 300 series have peak drag uncertainties of +18% to -13%, +6% to -7% and +30% to -12% respectively.

5.3.3 Failure Velocity

For failure method A, the 300-series fails earlier than the other two block types as shown in Figure 20. Due to the reduced effect of drag force and the larger effect of lift on the stability analysis of method A, the minimum stability is pushed closer to 45º. As can be seen in Figure 20, the 400-series and 500-series blocks have similar earliest failure flow rates. This means that for the stability of method A, the 400-series' stability to size ratio is far higher than the other block types. Therefore, a block with the shape of the 400 series can be lighter for a particular flow rate.

The repeatability for the 300-series, 400-series and 500-series failure flow rate A is 1.61%, 2.04% and 0.29% respectively by comparing the difference between -15° and 15°. The 300-series has a failure flowrate A of 2.258m/s to 1.704m/s lower than the 400-series block (only between 0º and 45º, the other two incident angles are inconsequential to mattress failure). The 500-series has a failure flowrate A between 0.243m/s higher and 0.058m/s lower than the 400-series block (only between 0º and 45º, the other two incident angles are inconsequential to

mattress failure). The 500 series, 400 series and 300 series have peak failure flowrate A uncertainties of +6% to -8%, +5% to -8% and +4% to -8% respectively.

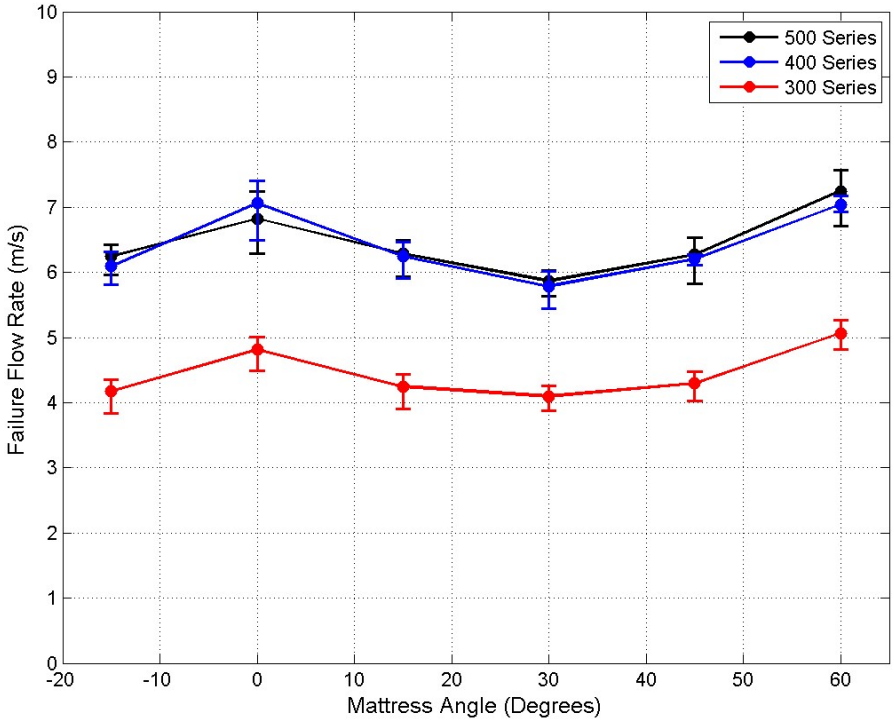

Figure 20: Failure flow rate for the 300-series, 400-series and 500-series centre blocks, for failure method A.

For failure method B shown in Figure 21, the block types have far closer stabilities than method A shown in Figure 20. Like the 300-series block position comparison, all the block types have higher stability at larger angles due to the inverse relationship between the failure flow rates and the lift, drag and overturning moments.

Unlike failure method A, failure method B has more stable block types. The 400-series is more stable at all angles compared to the 500-series. This means that the effectiveness of the 500-series is based purely on stability and not cost. The 300-series is also a lot closer to the other block types and is a cheaper option to construct in industry.

The repeatability for the 300-series, 400-series and 500-series failure flow rate B is 1.95%, 1.08% and 0.22% respectively by comparing the difference between -15° and 15°. The 300-series has a failure flowrate B of 0.798m/s to 0.517m/s lower than the 400-series block (only between 0º and 45º, the other two incident angles are inconsequential to mattress failure). The 500-series has a failure flowrate B of 0.2660m/s to 0.1094m/s lower than the 400-series block (only between 0º and 45º, the other two incident angles are inconsequential to mattress failure). The 500 series, 400 series and 300 series have peak failure flowrate B uncertainties of +4% to -6%, +4% to -2% and +4% to -9% respectively.

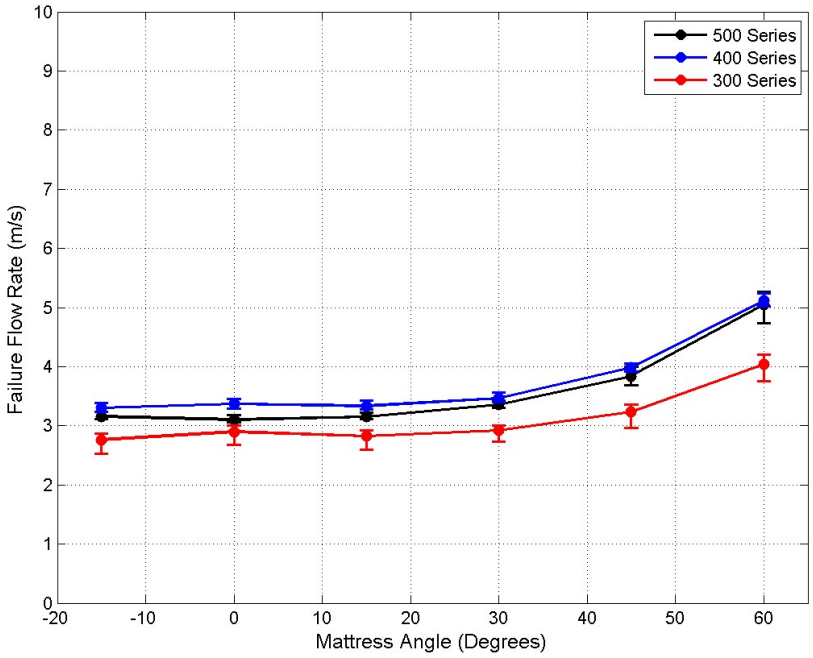

Figure 21: Failure flow rate for the 300-series, 400-series and 500-series centre blocks, for failure method B.

Chapter 6

6 Discussion

6.1 Introduction

The results of Chapter 5 are discussed in more detail in the following sections. Section 5.2 involved the identification of the initial failure location of the mattress, the results of which are further analysed in Section 6.2. By highlighting which mattress location has the lowest stability, further experimental investigations were able to be conducted on one block only, thereby reducing the amount of required data. Following this, the hydrodynamic characteristics of different block types are compared and discussed further in Section 6.3 to determine which block type has the highest stability. The resulting hypotheses are then verified using both experimental and numerical flow profiles in Section 6.4, followed recommendations for ACM shape optimisations.

6.2 Block Location Selection

The stability of the corner block and the centre block were compared on the leading-edge at all horizontal incident flow angles, to determine which block has the lowest stability. The results of the experiment showed that the centre block has the lowest stability, which can be attributed to various fluid mechanics including higher lift and lower drag. The causes of these are hypothesised and discussed in further detail below. The reduced lift seen by the corner blocks in comparison to the centre block can be attributed to the downwash effect. The downwash effect is where the pressure difference between the bottom face of an aeroplane wing and the top face of the wing is reduced through vortex shedding, as seen on plane wings using winglets.

This effect does not occur on the centre blocks due to the adjacent blocks obstructing vertical fluid transmission, however it is a major factor in the reduced lift for the corner blocks.

The most likely reason the corner block has lower drag than the centre block in a perpendicular fluid flow is due to cross flow in front of the corner block caused by pressure relief at the exposed edge of the mattress. The corner block has higher flow rate on the open side of the block which causes a transverse pressure differential and therefore a transverse flow. The cross flow causes reduced pressure in front of the blocks. This reduces the longitudinal differential pressure and therefore reduces drag.

6.3 Block Type Comparison

This section discusses the different block types and how variations in block size affects mattress stability. Three different block types in six different flow angles were investigated, namely the 300-series, 400-series and 500-series. The hydrodynamic characteristics of each are further discussed in the following sections.

6.3.1 Coefficient of Lift

The results of the experiment showed that the 500-series has greater lift than the 300-series and 400-series, as seen in Figure 18. Therefore, the 500-series' increased lift is due to its larger bottom half and steeper face as shown in Figure 2. It is hypothesises that the steep bottom face causes reduced flow velocity and therefore increases pressure on the bottom half of the blocks, and hence increases lift.

Unlike the 500-series and the 400-series, the 300-series has a small top shell. By comparing the lift and resulting stability, the effect of changing shell size and location can be hypothesised. The 400-series has low lift relative to its size as it has equal or lower lift than the 300 series mattress, contributing to its higher overall stability. It can therefore be hypothesised that decreasing the size of the top shell has a little to no effect on lift. Unlike the bottom shell, the top is open to the free stream velocity which means that changes in the top shell will have minimal effect on flow velocity above the block and therefore will have minimal effect on the lift coefficient. It is important to note that increasing in the size of the top shell increases the weight of the block, therefore increases overall stability.

6.3.2 Coefficient of Drag

The results of the experiment show that the 500-series has a lower drag coefficient than both the 300-series and 400-series. Drag is caused by a longitudinal differential pressure, so drag can be affected by the pressure in front of the blocks and behind the blocks. While it is true that the increase in block size and the inherently steeper slope does increase the pressure in front of the blocks, it also increases flow separation behind the blocks and therefore increases pressure at the back of the blocks, resulting in higher overall drag for the larger 500-series blocks. This increased pressure is amplified by the steep front face of the second row of blocks, which maintain the high pressure between the first and second row. This increase in rear pressure reduces drag and thus has a greater effect on the drag coefficient than the frontal pressure increases.

6.3.3 Failure Velocity

The 300-series has the lowest failure velocity, followed by the 400-series then the 500-series. Like the 300-series block position comparison, the major factor in the 300-series' relatively reduced stability is the negative effect of drag on the other two block types. For pivot point A, drag acts against the overturning moment and therefore increases stability. The drag for the 300-series is dramatically lower than the other two block types and therefore has reduced stability for failure method A.

The 500-series should only be used when more stability is needed than the 400-series can provide. However, a block with the same volume as the 500 series but with the top shell to bottom shell height ratio of the 400 series will be hypothetically more stable than the existing 500 series ACM. The 300-series however is cheaper to construct than the other blocks due to its symmetrical shape and small size. However, the 300 series has lower stability than the other two mattresses. Therefore, the 300-series should only be used in low current areas.

6.3.4 Limitations

The main component of ACMs that has not been accounted for in this research is scour propagation around and between the blocks. It is possible that although the 500-series has lower stability and costs more, it could reduce scour propagation. This means that for specific situations, for example an ACM on fine silt, it may be viable to use the 500-series over the 400-series.

6.4 Three-Dimensional Flow Profiling

Through experimental and numerical flow profiling, this section aims to verify several hypotheses made about the flow around ACMs in the previous results sections of this thesis. These verifications will allow for further optimisation of ACM block shapes. The previous sections both made major flow hypotheses during their analysis. To prove that these hypotheses are realistic, flow streamline tests were conducted both experimentally and numerically. Please note that all credit for the numerical results used within this thesis are credit to Hung (2016). Hung's paper (Hung, 2016) goes in depth into his numerical study into ACM hydrodynamics. Hung (2016)'s work is used here purely for comparative purposes, all credit for the work goes to the author.

6.4.1 Block Location Flow Analysis

To further understand ACM stability, it is not enough to simply know the lowest stability location. We must also investigate the variations in flow that cause these changes in stability. Section 5.2 hypothesised that the source of the increased stability at the corner block is due to the pressure release along the front and side of the block. The exposed side of the block causes these variations in pressure by allowing the fluid in front and along the side of the block to access the free stream velocity. The access to a lower pressure zone causes a vertical flow beside the block as shown in Figure 22 and cross flow in front of the corner block, as seen in Figure 23. The reduction in pressure is mostly located at the bottom half of the block due to the stagnation that occurs there. This means that the cross flow reduces both the lift and the drag.

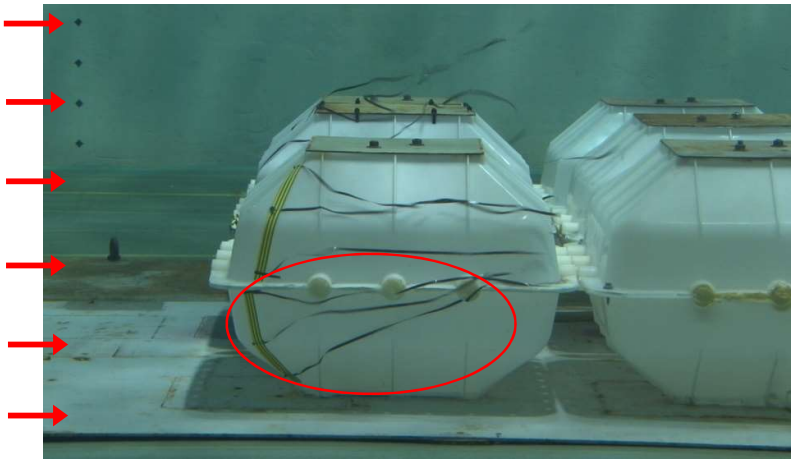

Figure 22: Experimental streamlines. 300-series at a flow angle of 15 degrees and a flow velocity of 0.4m/s.

Figure 23 has several significant impacts for this thesis, it shows the horizontal pressure relief in the form of a cross flow in front of both corner blocks, validates the horizontal pressure relief hypothesis made in Section 5.2 and it also shows a smaller amount of pressure relief caused by the gaps between the blocks, as visualised through the movement of the streamlines in front of the centre block.

The other pressure relief mechanism is the vertical pressure relief at the side of the block. Due to the exposed side of the block, the pressure difference between the top and bottom of the block is balanced due to an upwards fluid flow. This decreases the lift dramatically in comparison to the centre block, which has the fluid on the bottom half of the block completely separated from the top half. The vertical pressure relief is a common fluid dynamics phenomenon discussed by aeronautical engineers. For example, due to the reduction in lift at the end of a plane's wing, winglets were invented. Figure 22 clearly shows an upwards flow at the side of the block. This flow is mainly located at the bottom of the block because of pressure

balancing between the high pressure under the block and the low pressure above the block. Figure 22 proves the vertical pressure relief hypothesis made in Section 5.2.

In order to validate the experimental streamlines, a computational investigation was undertaken by Hung (2016). Figure 24 and Figure 25 show his work and validate the experimental findings found in Figure 22 and Figure 23 respectively. These validations are also useful for validating the computational analysis method which allows for its use in more complex streamline studies.

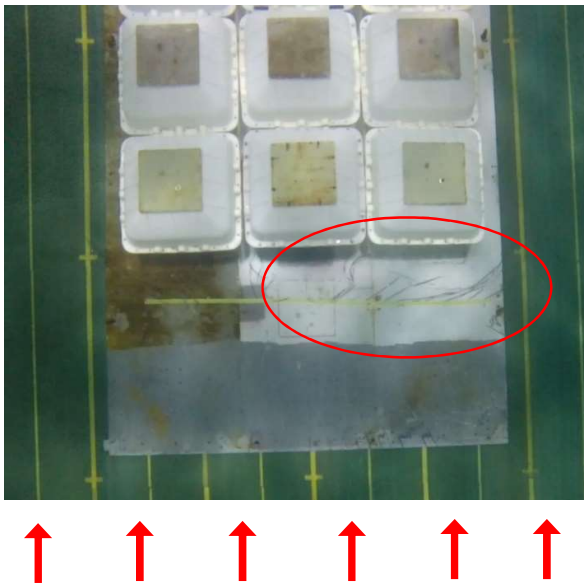

Figure 23: 300-series streamlines, top view. The mattress is in a flow angle of 0 degrees and a flow velocity of 1.6m/s.

6.4.2 Flow Analysis Around Varied Block Types

Once the failure location was found, block shape optimisation could be investigated. Section 5.3 investigated the stability of ACM block types that are currently used in industry. The block types that were investigated were the 300, 400 and 500-series made by Subcon Technologies. The 2D flow profiles for the 300-series, 400-series and 500 series are shown in Figure 26 (a), (b) and (c) respectively.

The computational method was used due to the complexity of this study. It is difficult to make experimental streamlines stay off the surface of the block without disturbing the flow. Therefore, mid fluid streamlines cannot be found experimentally.

The main findings of Section 5.3 was that the 400-series has the highest stability when compared to the 300-series and 500-series. This is relevant because the 400-series has a lower

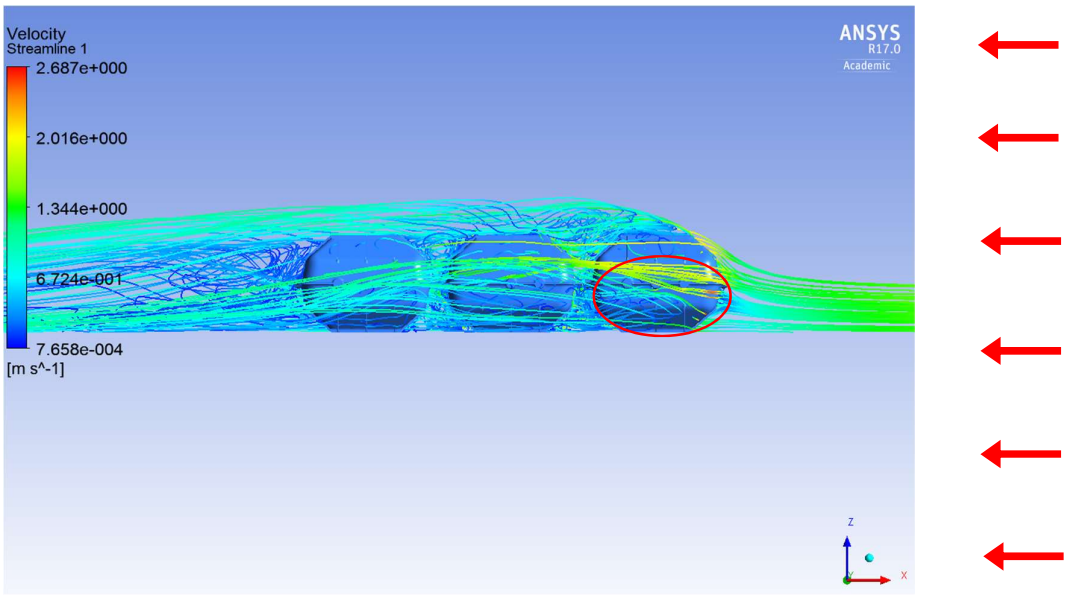

Figure 24: 300-series streamlines, side view. The mattress is in a flow angle of 0 degrees and a flow velocity of 1.6m/s. (Hung, 2016)

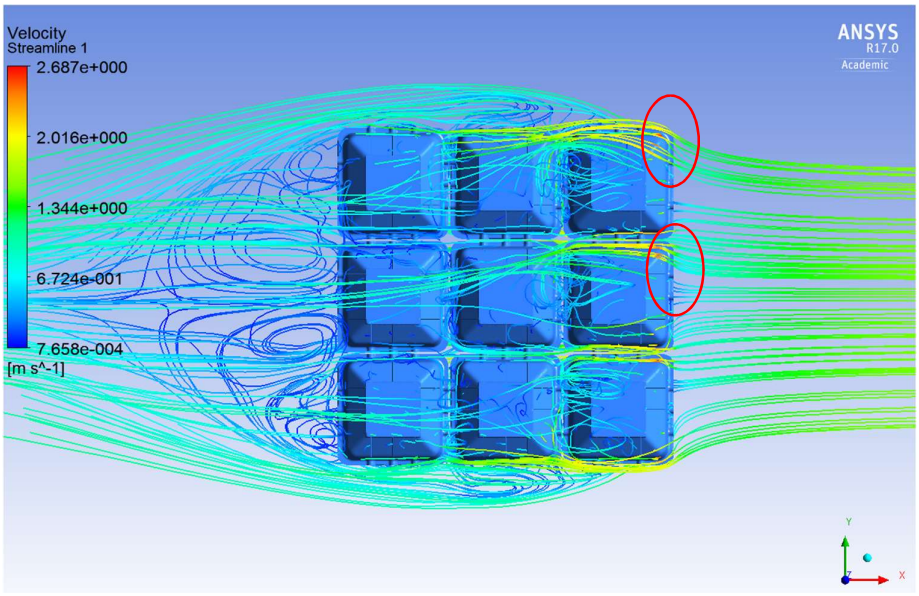

Figure 25: 300 Series streamlines, top view. The mattress is in a flow angle of 0 degrees and a flow velocity of 1.6m/s. (Hung, 2016)

construction cost and higher stability than the 500-series. With the 400-series having a high cost to stability ratio, it is important to find out what causes its increased stability. It is possible that understanding why the 400-series is so stable could allow for further block optimisation.

In Section 6.2, the flow was assumed to be completely separated at the join between the halves of the blocks. Therefore, it can be assumed that there is no pressure relief between the two halves of the centre block. This assumption cannot be used for the corner block as previously discussed. Due to the findings of Section 5.2, only the centre block is investigated further, allowing for the assumption to be made. The purpose of this assumption is to allow for the simplification of the force analysis. Due to the assumption that the fluid mechanics are independent above and below the connection between the two halves of the block, the force can be independently analysed for the top and bottom half of the block.

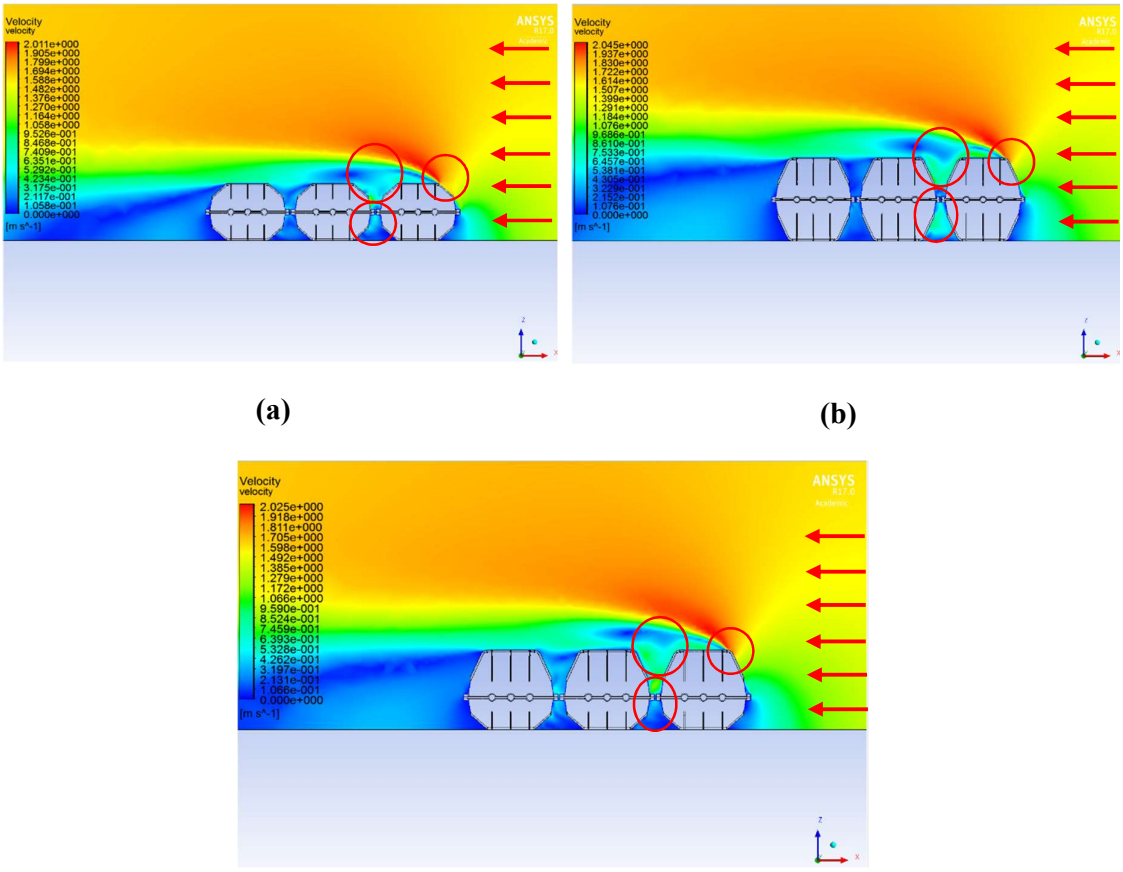

Figure 26 : Flow comparison between different block types. (a) 300-series, (b) 500-series and (c) 400-series. All block types have a flow angle of 0 degrees and a flow velocity of 1.6m/s. (Hung, 2016)

Section 6.3 hypothesised that increasing the top shell's size will increase the pressure at the front of the block. However, it will also increase separation at the back of the block, causing an increase in backpressure, which reduces drag and lift. The row of blocks behind the leading edge also increases the passive fluid pressure behind the leading-edge block, therefore reducing both drag and lift. Figure 26 (a) and (b) both show a turbulent zone behind the larger block types. This turbulent zone occurs in the higher velocity zone behind the block and beneath the

low velocity laminar separation point at the top of the block. However, turbulent zones cannot be simply analysed using Bernoulli's principle. While turbulence may increase fluid velocity, hence decreasing the pressure, the turbulent nature also increases the pressure on the surface of the block. These counteracting pressure effects balances the pressure on the back of the block, so that the top shell and bottom shell have roughly the same pressure for all block types.

While the hypothesis as stated in Section 6.3 is inaccurate in estimating that there would be a larger backpressure for the larger block, the pressure did not very much. However, although Section 6.3's hypothesis is accurate for the front of the block due to the flatter angle of the smaller shell (Figure 26 (a)), there is a higher flow rate at the top shell's front face. The increased velocity shown in Figure 26 (a)reduces both the pressure of the fluid, causing a reduced form-drag, and the change in momentum, causing dramatically reduced interference drag.

Section 6.3 also hypothesised that due to the isolation of the fluid around the bottom shell from the free stream, the back of the block will also have high stagnation. This reduces the drag caused by the bottom shell for both the large and small shells. However, this would primarily affect the larger shell. Section 6.3 is correct in saying that the bottom shell would have high pressure. However, from the CFD results presented here, the smaller shell is only affected by a small amount compared to the larger shell. They have almost identical flow rates, as shown in Figure 26, and therefore almost identical pressures. Unlike Section 6.3's hypothesis, it is in fact the top shell's pressure that is affected dramatically by block size.

Section 6.3 hypothesised that the smaller block size has less separation and therefore has lower top pressure, which increases lift. As stated previously, Section 5.3 neglected to consider the effect of turbulence and therefore the top of the block has higher pressure than what Bernoulli's

principle implies. With turbulence realistically modelled, there is only a small uplift created at the back of the block for all block types.

With the back of the block generating minimal lift, the front of the block must be where the 400-series gains its high stability. The 300-series has low stability due to the low pressure on the front of the top shell as discussed earlier. While all the block types have similar bottom shell pressures, the 400-series has one significant advantage. In comparison to the 500-series, the 400-series has the same top and bottom pressure. However the 400-series has a far lower bottom area. Due to lift being a force and not a pressure, this reduced bottom area decreases the 400-series' lift dramatically.

6.4.3 Block Shape Optimisation

To increase the cost efficiency of each block type, the block shape can be hydrodynamically optimised. This hydrodynamic optimisation aims to increase the stability of the block and therefore reduces the required weight of the block for a specific flow rate.

This section assumes that the generic shape of the previously investigated block types remains the same. This means that the block shape remains symmetrical about the vertical axes.

Due to this symmetry, the main optimisations that can be made are based on lift. As previously discussed, lift is largely linked to the leading-edge of the block. The 400-series has reduced lift due to its shear top face, which increases the top pressure and creating a larger downforce. The 400-series also has a smaller bottom area, which reduces the force acting on the bottom shell by reducing the area component of a simple pressure equation.

This reduction in the bottom area is effective. However, it is only one component in the force equation, with the other component being pressure. To reduce the bottom pressure, a more streamline bottom shell must be created. Figure 27 shows an option for increasing the hydrodynamic efficiency for an ACM's bottom shell. This shape will reduce the pressure on the bottom shell dramatically and therefore reduce lift. This shape optimisation can be roughly defined by comparing a circle's drag coefficient of 1.2 to a square's drag coefficient of 2.05. This comparison roughly approximates the difference in pressure between the differing shapes of the bottoms of the blocks.

Another way of reducing bottom shell pressure is through the use of a pressure relief system. Pressure relief is discussed in Section 6.2 and is the main reason the corner block has higher stability than the centre block. By using a piping system from the front of the block to the back of the block, this could result in a dramatic reduction in bottom pressure.

While it is possible or even likely that a different shape would be more stable, further research is necessary to determine what further shape optimisations can be made.

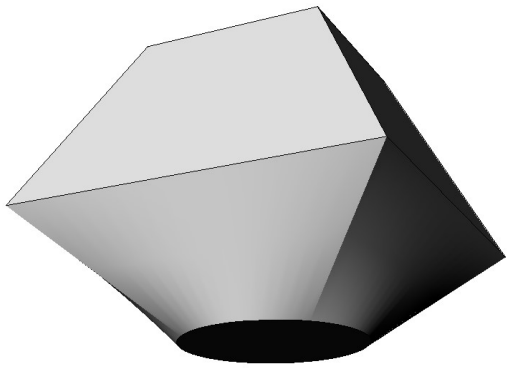

Figure 27: Block shape optimisation suggestion. Modified 400 series with a hydrodynamically efficient bottom shell.

Further optimisations could also be made to the mattress arrangement. As discovered earlier, the second row of 500-series blocks decreases the overturning moment due to a reduction in top drag. It is possible that a more efficient arrangement would be a 300-series leading edge with a 400-series second row. Further research is required to validate this hypothesis.

Another weakness of the ACM design is its 'negative static stability', which causes a reduction in its stability as soon as the mattress is lifted off the ground. This negative static stability is caused by an increase in lift due to the increased bottom pressure, therefore lifting the centre of drag and increasing the overturning moment. Therefore, the maximum stability of an ACM is equal to their static stability. To improve their stability, a design which ensures a 'positive static stability' would be effective. Due to the ACM's ability to trench the leading edge into the ground, a positive static stability design would cause the leading edge of the mattress to lift and resettle repeatedly. This would entrench the leading edge and result in gains in ACM stability. This could be possible through pressure relief on the bottom face of the leading-edge blocks, for example a piping system from the bottom face to the back or to the top face of the block. This shape optimisation would require extensive further testing.

Chapter 7

7 Conclusions

Three main research questions were investigated within this thesis. Section 5.2 investigated the stability of a full mattress and how the block position within the mattress affects the stability of the block for different flow angles. Section 5.3 considered the effect of block type on mattress stability and recommended existing block types with maximum stability. Section 6.4 investigated local hydrodynamic effects around the blocks and linked these effects to the stability of the mattresses found in the previous two sections. Section 6.4 recommended block and mattress optimisations using the knowledge obtained in Section 5.2, Section 5.3 and further research into localised ACM hydrodynamic effects.

Three different experimental investigations were undertaken during this thesis. Section 5.2 investigated ACM failure locations by comparing the leading-edge centre block to the leading-edge corner block. The location comparison used the 300-series ACM as the base model. Section 5.3 used the main failure location found from Section 5.2 to compare the 300-series to the 400-series and 500-series ACM types. Section 6.4 investigated fundamental ACM flow mechanics to recommend ACM shape optimisations. Each of these investigations used the methodology and model structure developed by Francis (2013). Francis (2013)'s methodology was further developed through the novel components of changing the mattress array to a 3 by 3 mattress to allow for centre block studies, and by introducing cross talk calibrations for increased accuracy.

From Section 5.2 it was found that for failure method A, the corner block does not have an earlier loss of stability than the centre block. Therefore, the failure of the full mattress is purely based on the centre block's loss of stability. Method B has a corner block stability slightly lower than that of the corner block for angles above 40º. There is only a small difference between the two block positions and due to the failure method that requires the corner block to fail simultaneously with the centre block next to it, it is assumed that the corner block has negligible effect on stability loss for the full mattress.

Following the conclusion of Section 5.2, it is assumed that only the centre block of the other block types is needed to be tested in further investigations. This allowed for more thorough testing of the centre blocks in Section 5.3, which compares the 300-series, 400-series and 500-series mattresses. Based on this study, it is recommended that future ACM investigations outside of this thesis consider only the centre block in the leading edge. It is recommended that the mattress should be at least 3 blocks wide and at least 2 blocks long. However, if a study with only 2 blocks long is conducted a sensitivity study should be conducted to check for variations between a 2 and 3 block long mattress.

In Section 5.3 of failure method A, the 300-series has far lower stability than the other block types. The 300-series is economically suitable for low flow rate areas due to its comparatively low cost. The interesting block type comparison is between the 400-series and 500-series. The 400-series has almost the same stability as the 500-series even though it has less weight. The 400-series failed 0.02 m/s earlier than the 500-series, which is effectively negligible, but the 400-series is far cheaper and therefore more cost effective. Due to the negligible difference between the 400 and 500-series, there is no reason from a stability and economic standpoint to use the 500-series. However due to the diverse uses for ACMs, the 500-series will still be useful

when extra weight is needed, for example to stabilise a subsea structure which is generating its own lift.

The 400-series' stability is even more prominent when using stability method B instead of method A. Using method B, the 400-series had higher stability than the 500-series and therefore the 500-series is redundant when compared to the 400-series. This difference is due to the 400-series' half shell efficiency. From this research, it was found that a large top half and a small bottom half is the most stable block form.

Section 6.4 of this thesis investigated how the three-dimensional flow profile around the blocks affected the hydrodynamic coefficients found in Sections 5.2 and 5.3. The block location comparison in Section 5.2 found that the corner block has higher stability than the centre block. By thoroughly investigating the flow mechanism that causes the corner block to have higher stability, it was found that the increase in stability is due to pressure relief from the downwash effect.

Recommendations for possible optimisations to ACM block shapes were found. From the investigation into flow variations based on block location, it is discovered that a major reduction in lift and drag can be achieved by creating pressure relief. This can be achieved by casting pipes in each block to pipe fluid between the bottom half of the blocks and the top.

From the block type comparison in Section 5.3 it was found that the rear half of the blocks has a limited effect on ACM lift, concluding that most of the block failure is caused by pressure on the front face of the block. The size of the bottom shell has limited effect on the pressure acting on the front of that shell. However, it was found that the main cause for the 400-series' high stability is due to its small bottom area relative to its large boxy top area, which decreases lift

on the 400-series. Reducing the block's bottom area is effective at reducing lift. However, further hydrodynamic optimisation can be obtained by reducing bottom pressure. To reduce the bottom pressure, a more streamline bottom shell must be created. Figure 27 shows an option to make the ACM's bottom shell more streamline. The shape of the block in Figure 27 will reduce the pressure on the bottom shell dramatically and therefore reduce lift.

Another method to reducing the bottom shell pressure is the use of a pressure relief system. Pressure relief is discussed in conjunction with Section 6.2 and is the main reason the corner block has higher stability than the centre block. By using a piping system from the front of the block to the back of the block, this could cause a dramatic reduction in bottom pressure.

Another weakness of the ACM design is its 'negative static stability', which causes a reduction in its stability as soon as the mattress is lifted off the ground. To improve ACM stability, a design which ensures a 'positive static stability' would be effective at maintaining stability even after losing static stability. This is possible through pressure relief on the bottom face of the leading-edge blocks, such as a piping system from the bottom face to the back of the block or to the top face of the block. This shape optimisation would require extensive further testing.

It is recommended that further testing be conducted in pressure relief systems and their effect on ACM stability. Once an effective design has been established, a full-scale dynamic test would be most effective for investigating how pressure relief methods effect ACM positive static stability.

References

AMC. (n.d.). *Circulating Water Channel*. Retrieved October 26, 2015, from Australian Maritime College: https://www.amc.edu.au/maritime-engineering/circulating-water-channel

Arzaghi, E. (2014). Numerical Investigation of Hydrodynamic Characteristics of High Performance Articulating Concrete Blocks Used in design of Alternative Revetments for a Ro-Ro Ramp. *Unpublished Article*.

Carnovale, R. (2014). Experimental Study into the Impact of Propeller Wash on an Articulating Concrete Block (ACB) Revetment System. *Unpublished Article*.

Chrenowski, T. H. (2014). Experimental study into the stability of SUBCON high performance. *Unpublished Article*.

Deng, L., & Cai, C. (2010). Bridge Scour: Prediction, Modeling, Monitoring, and Countermeasures-Review. *Journal of Hydraulic Engineering*, 125–134.

Det Norske Veritas. (1988). *RP E305 On-Bottom Stability Design of Submarine Pipelines.*

Det Norske Veritas. (2007). *RP-109 On-Bottom Stability Design of Submarine Pipelines.*

Dunlap, S. (2001). *Design Manual for Articulated Concrete Block Systems.* Harris County Flood Control District.

Francis, J. A. (2013). Experimental Study of Hydrodynamic Force Acting on a Concrete Mattress in Current. *Unpublished Article*.

Fredsøe, J. (2016). *Pipeline–Seabed Interaction (Doctoral dissertation).* American Society of Civil Engineers.

Godbold, J., Sackman, N., & Cheng, L. (2014). Stability Design for Concrete Mattresses. *International Society of Offshore and Polar Engineers*.

Griggs, R. (2014). *3D CFD Investigation of Hydrodynamic Forces on Subsea Articulated Concrete Mattresses.* Perth: International Society of Offshore and Polar Engineers.

Gyr, A., & Bewersdotff, H. W. (1995). Drag Reduction of Turbulent Flows by Additives. In H. W. A. Gyr, *Drag Reduction of Turbulence* (pp. 69-99). Springer Netherlands.

Hales, L. Z. (1980). *Erosion control of scour during construction.* Vicksburg Mississippi: US Army Engineer Waterways Experiment Station.

Hung, V. L. (2016). Investigating Hydrodynamic Characteristics of an Articulating Concrete Block by Applying Computational Fluid Dynamics (CFD). *Unpublished Article*.

Kjeldsen, S. P., Gjorsvik, O., Bringaker, K. G., & Jacobsen, J. (1973). Local scour near offshore pipelines. *Second International Conference on Port and Ocean Engineering Under Arctic Conditions (POAC)*, (pp. 27-30).

Klomp, W. H., Hansen, E. A., Chen, Z., Bijker, R., & Bryndum, M. B. (1995). Pipeline seabed interaction, free span development. *The Fifth International Offshore and Polar Engineering Conference.* International Society of Offshore and Polar E.

Knight, M., & Noyes, R. W. (1929). *Wind Tunnel Pressure Distribution Tests on a Series of Biplane Wing Models Part III. Effect of Changes in Various Combinations of Stagger, Gap, Sweepback and Decalage.* Washington: National Technical Information Service.

Lagasse, P. (2007). *Countermeasures to Protect Bridge Piers from Scour.* Transportation Research Board.

Langevin, G. S., & Overbey, P. (2003). *"To Reality: Winglets".* NASA Langley Research Center.

Lau, S. (2014). Numerical Investigation of the Effect of a Marine Propeller's Flow acting on High Performance Articulating Concrete Mattress as Revetment on a Ro-Ro Ramp. *Unpublished Article*.

Lillycrop, W. J., & Hughes, S. A. (1993). *Scour hole problems experienced by the Corps of Engineers.* COASTAL ENGINEERING RESEARCH CENTER VICKSBURG MS.

Lim, Y. F. (2013). Numerical Modelling of Hydrodynamic Forces acting on Concrete Mattress Blocks in Current. *Unpublished Article*.

Lucassen, R. J. (1984). *Scour underneath submarine pipelines.* TU Delft, Civil Engineering and Geosciences, Hydraulic Engineering.

McColl, M. (2016). Experimental Investigation Of An Articulated Concrete Mattress With Varied Flow Angle Of Incidence. *Unpublished Article*.

McLaren, R. W. (2014). Experimental Study Into the Effects of Propeller Wash on Concrete Mattress Revetments. *Unpublished Article*.

McLaren, R. W., Chin, C., Joshua, W., Jonathan, B., & Ranmuthugala, D. (2017). Articulated Concrete Mattress Flow Based Shape Optimisation. *Unpublished Article*.

McLaren, R. W., Christopher, C., Weber, J., Binns, J., & Ranmuthugala, D. (2016). Investigation of Hydrodynamic Forces on Location Based Leading Edge Articulated Concrete Blocks. *Unpublished Article*.

McLaren, R. W., Jasmin, M. B., Chin, C., Binns, J., Weber, J., & Allen, M. (2016). Articulated Concrete Mattress Block Size Stability Comparison in Omni-directional Current. *Oceans' 16.* Monteray: IEEE Oceanic Engineering Society.

Melville, B. W., & Coleman, S. E. (2000). *Bridge Scour.* Auckland New Zealand: Water Resources Publications, LLC.

NASA. (n.d.). *Downwash Effects on Lift*. Retrieved September 10, 2015, from National Aeronautics and Space Administration: https://www.grc.nasa.gov/www/K-12/airplane/downwash.html

National Concrete Masonry Association. (2010). *Design Manual for Articulating Concrete Block (ACB) Revetment Systems Second Edition.* Herndon: NCMA.

Neville, A., McLaren, R., Weber, J., Chin, C., Binns, J., & Taylor, A. (2016). Experimental Investigation Into The Effects Of Reduced Vertical Centre Of Gravity Of An Articulated Concrete Mattress In Current Flow. *International Journal of Maritime Engineering*.

Schrand, D. (n.d.). *CROSS-TALK COMPENSATION USING MATRIX METHODS.* Retrieved April 12, 2018, from HITEC Sensor Developments: https://www.hitecsensors.com/technical/cross-talk-compensation-using-matrix-methods/

Seabed Technologies LLC. (n.d.). *Welcome to Seabed Technologies, LLC*. Retrieved May 6, 2016, from Seabed Technologies, LLC: http://www.seabedus.com/

Shirhole, A. M., & Holt, R. C. (1991). Planning for a comprehensive bridge safety program. *Transportation Research Record 1290*, 39-50.

Sumer, B. M., & Fredsøe, J. (1990). Scour below pipelines in waves. *Journal of waterway, port, coastal, and ocean engineering*, 307-323.

Sumer, B. M., & Fredsoe, J. (1991). Onset of scour below a pipeline exposed to waves. *The First International Offshore and Polar Engineering Conference.* International Society of Offshore and Polar Engineers.

Sumer, B. M., & Fredsøe, J. (2002). *The Mechanics of Scour in the Marine Environment.* World Scientific Publishing Co.

Sumer, B. M., Jensen, H. R., Mao, Y., & J, F. (1988). Effect of lee-wake on scour below pipelines in current. *Journal of Waterway, Port, Coastal, and Ocean Engineering*, 599-614.

Sumer, B. M., Truelsen, C., Sichmann, T., & Fredsøe, J. (2001). Onset of scour below pipelines and self-burial. *Coastal engineering*, 313-335.

Taylor, A. (2016). Experimental Investigation Into The Effects Of Current Flow On An Articulated Concrete Mattress Of The ‘Half Block’ Arrangement. *Unpublished Article*.